Rev. Mexicana Astron. Astrof., 13, 9-14 (1986)

ON THE VERTEX DEVIATION OF YOUNG STARS

L.P. Bassino[1], V.H. Dessaunet[2], and J.C. Muzzio

Facultad de Ciencias Astronómicas y Geofísicas
Universidad Nacional de La Plata,
and Programa de Fotometría y Estructura Galáctica, CONICET
Argentina

Received 1985 July 15

RESUMEN

Se muestra que la desviación del vértex de estrellas jóvenes es una consecuencia natural del carácter epicíclico de los movimientos estelares en la galaxia. Si las estrellas son suficientemente jóvenes (edades del orden de 1.8×10^7 años), la desviación del vértex es de alrededor de $-30°$ y no resulta muy afectada por la formación de estrellas en un brazo o por las velocidades sistemáticas en el momento de su nacimiento; las estrellas de edades mayores (edades del orden de 6.5×10^7 años) sufren los efectos de modelado de sus condiciones de nacimiento.

ABSTRACT

We show that the vertex deviation of young stars is a natural consequence of the epicyclic character of the stellar motions in the galaxy. If the stars are young enough (ages of about 1.8×10^7 years), the vertex deviation is about $-30°$ and it is not much affected by the formation of stars in an arm or their systematic velocities at birth; older stars (ages of about 6.5×10^7 years) suffer the modelling effects of their birth conditions.

Key words: GALAXY-STRUCTURE

I. INTRODUCTION

The elementary theory of stellar systems with rotational symmetry shows that if the distribution of peculiar stellar velocities is ellipsoidal, then the longest axis of the velocity ellipsoid (i.e. the vertex direction) should point toward the galactic center (see, e.g. Ogorodnikov, 1965). This prediction agrees with the observational results for old stars, but young stars exhibit an appreciable vertex deviation in the plane of the Galaxy. See, e.g. Delhaye (1965), for a general review of the subject, Nordström (1936) and Filin (1957) for the particular case of the young stars.

Several authors attempted to explain the vertex deviation within the framework of theories that predict regions of star formation, like spiral arms, and the velocities the stars have when they are born. Among others, we can mention the work of Yuan (1971) and of Hilton and Bash (1982); the latter used the observational results of Filin (1957) for comparison. While these attempts are interesting, in the present paper we want to sound a word of caution regarding the use of the vertex deviation as a check for theories. Using the epicyclic approximation, we show that the vertex deviation is just a natural consequence of the stellar motions in the galaxy (section II) and then, in section III, we present simple numerical models to explore the limits of our analytical derivations; in section IV we discuss the different causes that affect the vertex deviation for young stars, and in section V we summarize our results.

1. On a fellowship from the Consejo Nacional de Investigaciones Científicas y Técnicas de la República Argentina.
2. On a fellowship from the Comisión de Investigaciones Científicas de la Provincia de Buenos Aires.

II. A SIMPLE ANALYTICAL THEORY

As we are interested in the motions of young stars, whose orbits do not depart too much from circles, it is reasonable to use the epicyclic approximation for the present investigation; Woolley (1970) also used that approximation to investigate the vertex deviation, but he was interested in stars older than those we will deal with.

Adopting the usual convention for the coordinates in the rotating frame of reference, ξ and η, and the residual velocities, u and v, we have (see, e.g., Lindblad 1959):

$$\xi = C_1 + C \cos \kappa (t - t_0) \quad (1)$$

$$\eta = -2 A C_1 (t - t_1) - C (\omega/-B)^{1/2} \sin \kappa (t - t_0) \ , \quad (2)$$

$$u = -C \kappa \sin \kappa (t - t_0) \ , \quad (3)$$

$$v = 2 B C \cos \kappa (t - t_0) \ ; \quad (4)$$

where t is time, ω is angular speed, κ is epicyclic frequency, A and B are Oort constants near the Sun, and C, C_1, t_0 and t_1 are parameters of the orbit.

Let us set $t = 0$ at present and $t = -\tau$ at the time the stars were born. As the stars we observe lie now near the Sun, we have:

$$0 = C_1 + C \cos \kappa t_0 \ , \tag{5}$$

$$0 = 2 A C_1 t_1 + C (\omega/-B)^{1/2} \sin \kappa t_0 \ ; \tag{6}$$

and if the components of the velocity of the star at birth are $(-V \cos l, V \sin l)$, then:

$$-V \cos l = C \kappa \sin \kappa (\tau + t_0) \ , \tag{7}$$

$$V \sin l = 2 B C \cos \kappa (\tau + t_0) \ . \tag{8}$$

Solving the system of the equations (5) through (8) we obtain the orbital parameters which, substituted in equations (1) through (4) allow us to obtain the present stellar velocity:

$$u_0 = -V \cos l \cos \kappa\tau - (\kappa V \sin l \sin \kappa\tau)/2B \ , \tag{9}$$

$$v_0 = V \sin l \cos \kappa\tau - (2 B V \cos l \sin \kappa\tau)/\kappa \ ; \tag{10}$$

and the stellar position at birth:

$$\xi_{-\tau} = [V (1 - \cos \kappa\tau) \sin l]/2B + (V \sin \kappa\tau \cos l)/\kappa \ , \tag{11}$$

$$\eta_{-\tau} = -(\omega/-B)^{1/2} V (1 - \cos \kappa\tau) \cos l/\kappa + \\ + 2 A \tau V \cos l \sin \kappa\tau/\kappa - \\ - A \tau V \sin l \cos \kappa\tau/B + \\ + (\omega/-B)^{1/2} V \sin l \sin \kappa\tau/2 B \ . \tag{12}$$

It is easy to see that formulae (9) and (10) define an ellipse, whose axes point in the directions $l_{1,2}$ given by:

$$\operatorname{cotg} 2l_{1,2} = [(\kappa^2 + 4B^2) \operatorname{tg} \kappa\tau]/4B\kappa \ . \tag{13}$$

In other words, if we assume that the stellar velocities have the *circular* velocity distribution, equations (7,8) when the stars are born, later on they acquire the *elliptical* velocity distribution, equations (9) and (10), whose vertex deviation is given by formula (13).

The vertex deviation of stars just born ($\tau = 0$), defined as a limit because the velocity distribution is circular, is $-45°$ ($B < 0$); if we consider older stars, the vertex deviation diminishes (in absolute value) reaching $0°$ for $\tau = \pi/2\kappa$, when the ratio of the semiaxes reaches a value of $4B^2/\kappa^2 \cong 0.4$, and then acquires positive values reaching a maximum of $+45°$ for $\tau = \pi/\kappa$, when the distribution is circular again.

Figure 1 shows the velocity ellipse of equations (9) and (10) for $V = 10$ km s^{-1} and $\tau = 10^7$ y; the vertex deviation is $l = -35°$ and the minor and major semiaxes are 8.6 km s^{-1} and 11.6 km s^{-1}, respectively.

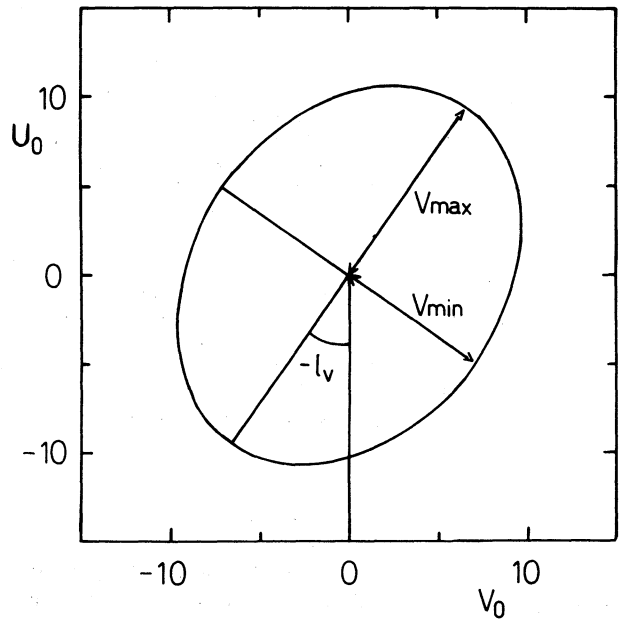

Fig. 1. Velocity ellipse given in equations (9) and (10) for V = 10 km s^{-1} and $\tau = 10^7$ y; the vertex deviation is $l_V = -35°$ and the minor and major semiaxes are 8.6 km s^{-1} and 11.6 km s^{-1}, respectively.

The model is too simple, and we will not push its consequences farther, but we note that it allows us to explain the large negative vertex deviation of very young stars, and the decreasing deviation and the increase in the ratio of the semiaxes of the velocity ellipse for older stars, as mere consequences of the epicyclic motion of the stars in the galaxy.

III. NUMERICAL MODELS

Several objections can be raised about the naive analysis of the previous section. To begin with, stars of a given spectral type and luminosity class do not have all the same age, but rather they have ages that span from zero to τ years. Besides, although it is reasonable to accept a spheroidal velocity distribution for the stars just born, different velocities have different probabilities: the larger the velocity the smaller the probability; the effect of sys-

tematic motions, in addition to the random ones, has not been considered either. Also, not all the stars used for kinematical studies lie in the immediate solar neighborhood; allowance for at least a few hundred parsecs should then be made in formulae (5) and (6). Finally, formulae (11) and (12) imply that the stars had to be born in certain places (again an ellipse) and, if stars were not born τ years ago in *all* those places, then the velocity ellipse given by equations (9) and (10) would be deformed, because parts of it would be lacking.

The effect of the systematic motions is the easiest to evaluate. If in formulae (7) and (8) we add, respectively, systematic terms u_i and v_i to the first members, it follows simply that in formulae (9) and (10) additional terms appear which are respectively:

$$\Delta u_0 = u_i \cos \kappa\tau - (\kappa/2B)\, v_i \sin \kappa\tau \qquad (14)$$

and

$$\Delta v_0 = (2B/\kappa)\, u_i \sin \kappa\tau + v_i \cos \kappa\tau. \qquad (15)$$

These terms change with stellar age, τ, but they are independent of longitude; therefore, the systematic motions of stars at birth have no direct incidence on the vertex deviation. They could, however, have some indirect effect because, for example, they also change the positions given in formulae (11) and (12) where the stars originated.

The most likely result of the other effects is probably a softening, or blurring, of the clear-cut results of the previous section and, as long as the stars are young enough, the main trends should not be much altered. For example, if we consider velocities of about 10 km s^{-1}, stars younger then 10^7 years could not have drifted more than 100 pc from their place of birth, and the modelling introduced by the presence of an arm about 1000 pc wide is probably irrelevant; alternatively, spectral types that include stars up to 10^8 years old would yield a mixture of negative and positive vertex deviations and, introducing thus, a considerable complication of our elementary scheme.

In order to obtain a quantitative check of the previous qualitative description we carried out some numerical simulations as follows. Every 10^6 years, and over a time span equal to the maximum stellar age, we generated a fixed number of stars, choosing at random their positions from a uniform distribution and their velocities from a circular Gaussian distribution. From those positions and velocities at birthtime we obtained, using the epicyclic approximation, the present positions and velocities; stars that lie at present within a given distance from the Sun were retained, and the others were rejected. We then used the final sample to derive the mean velocity and the parameters of the velocity ellipse (i.e. minimum and maximum velocity dispersions and vertex deviation).

Maximum stellar ages of 1.8×10^7 years or of 6.5×10^7 years were adopted for most models; the former corresponds to a spectral type of about B2.5, and the latter to one of about B5, according to the age scale adopted by Hilton and Bash (1982). A couple of models were run taking a maximum age of 13×10^7 years, a value large enough to yield a positive vertex deviation in

TABLE 1
PARAMETERS OF THE NUMERICAL MODELS

Model	Max. Age (10^7 y)	Radius Solar Neighb. (pc)	Region Star Formation	System u (km s^{-1})	System v (km s^{-1})
1	1.8	200	no limits	0	0
2	1.8	400	no limits	0	0
3	6.5	200	no limits	0	0
4	6.5	400	no limits	0	0
5	1.8	200	arm ($\xi > 0$)	0	0
6	1.8	400	arm ($\xi > 0$)	0	0
7	6.5	200	arm ($\xi > 0$)	0	0
8	6.5	400	arm ($\xi > 0$)	0	0
9	1.8	200	no limits	8	0
10	1.8	200	no limits	0	− 8
11	6.5	200	no limits	8	0
12	6.5	200	no limits	0	− 8
13	1.8	200	arm ($\xi > 0$)	8	0
14	1.8	200	arm ($\xi > 0$)	0	− 8
15	6.5	200	arm ($\xi > 0$)	8	0
16	6.5	200	arm ($\xi > 0$)	0	− 8
17	13.0	200	no limits	0	0
18	13.0	200	arm ($\xi > 0$)	0	0
19	1.8	200	no limits	8	− 8
20	6.5	200	no limits	8	− 8

TABLE 2
MEAN VELOCITIES AND PARAMETERS OF THE VELOCITY ELLIPSES

Model	⟨u⟩ (km s^{-1})	⟨v⟩ (km s^{-1})	σ_{max} (km s^{-1})	σ_{min} (km s^{-1})	$\sigma_{min}/\sigma_{max}$	l_v
1	0.6 ± 0.5	0.4 ± 0.4	9.3 ± 0.1	6.9 ± 0.2	0.74 ± 0.02	− 31.8 ± 6.4
2	0.5 ± 0.2	− 0.5 ± 0.9	9.5 ± 0.0	7.2 ± 0.1	0.76 ± 0.01	− 19.0 ± 6.9
3	0.6 ± 0.6	− 0.4 ± 0.1	11.1 ± 0.3	6.4 ± 0.2	0.58 ± 0.01	− 8.4 ± 1.2
4	− 0.6 ± 0.6	0.2 ± 0.3	11.7 ± 0.6	6.2 ± 0.1	0.54 ± 0.02	− 5.4 ± 0.5
5	− 3.0 ± 1.2	0.3 ± 0.5	8.8 ± 0.4	6.8 ± 0.2	0.78 ± 0.05	− 32.1 ± 1.0
6	− 1.7 ± 0.4	− 0.3 ± 0.3	9.5 ± 0.1	7.1 ± 0.2	0.75 ± 0.02	− 33.4 ± 8.6
7	− 6.9 ± 0.5	1.0 ± 0.2	9.4 ± 0.1	5.6 ± 0.1	0.59 ± 0.01	− 23.0 ± 2.7
8	− 5.9 ± 0.3	1.0 ± 0.0	9.7 ± 0.3	6.4 ± 0.0	0.67 ± 0.02	− 14.6 ± 5.0
9	− 3.9 ± 0.3	− 7.5 ± 0.7	9.8 ± 0.2	7.4 ± 0.1	0.75 ± 0.03	− 25.9 ± 10.4
10	6.7 ± 0.4	− 1.8 ± 0.6	9.3 ± 0.1	7.0 ± 0.2	0.76 ± 0.04	− 30.8 ± 1.5
11	− 9.2 ± 1.0	− 3.7 ± 0.1	11.3 ± 0.5	7.6 ± 0.0	0.68 ± 0.03	3.2 ± 3.7
12	3.5 ± 0.4	− 3.7 ± 0.2	11.8 ± 0.3	6.4 ± 0.4	0.54 ± 0.04	− 7.0 ± 2.0
13	− 6.4 ± 1.3	− 7.7 ± 0.7	8.6 ± 0.4	7.2 ± 0.2	0.83 ± 0.02	− 48.2 ± 8.7
14	2.8 ± 0.7	− 0.4 ± 0.2	8.7 ± 0.2	6.7 ± 0.4	0.77 ± 0.05	− 48.7 ± 11.5
15	− 12.7 ± 0.3	− 2.4 ± 0.2	10.2 ± 0.2	7.4 ± 0.3	0.73 ± 0.03	− 8.4 ± 3.7
16	− 6.6 ± 0.3	− 1.8 ± 0.5	10.5 ± 0.4	5.7 ± 0.1	0.54 ± 0.02	− 17.3 ± 3.8
17	− 0.4 ± 0.4	− 0.6 ± 0.2	10.6 ± 0.7	6.6 ± 0.4	0.62 ± 0.05	− 5.9 ± 2.6
18	− 3.6 ± 0.4	3.6 ± 0.2	10.0 ± 0.6	5.5 ± 0.2	0.56 ± 0.06	− 13.9 ± 1.8
19	4.4 ± 0.9	− 9.5 ± 0.8	9.6 ± 0.5	7.0 ± 0.4	0.73 ± 0.04	− 23.3 ± 7.3
20	− 4.7 ± 0.4	− 7.4 ± 0.4	12.2 ± 0.2	6.4 ± 0.2	0.53 ± 0.02	− 5.0 ± 2.2

our simple analytical model. The maximum radius for the solar neighborhood was also given two different values (200 pc and 400 pc), in different models, to check its effect on the kinematical properties.

Oort constants A and B were taken as 15 km s^{-1} kpc^{-1} and −10 km s^{-1} kpc^{-1}, respectively (Schmidt 1965); the velocity dispersion of the stars at birth was chosen as 8 km s^{-1}, a value similar to the one for gas clouds (see, e.g., Kerr 1968) and very young stars (see, e.g., Delhaye 1965).

The extension of the uniform spatial distribution of birthplaces was limited by the distance that a star would traverse, moving on a straight line with a speed equal to three times the velocity dispersion, in a time interval equal to the maximum stellar age. Thus, there is an extremely low probability that a star, whose velocity at birth follows the chosen law, reaches the solar neighborhood if it were born outside that region; in practice, this is equivalent to considering an unlimited region of star formation.

In order to obtain some insight into the influence of different conditions at birth, we also simulated stellar formation in a spiral arm limiting the birthplaces to the region with $\xi > 0$; the effect of systematic velocity components was investigated adding a constant value of 8 km s^{-1} in one or both coordinates to all the velocities at birth time.

Table 1 presents the different parameters and properties of the models. In each case, three different models were run keeping fixed those parameters and properties, and changing the seed number for the random number generator. Table 2 gives the mean values and root mean square error obtained in each case, from the three corresponding models, these are: the mean velocity components, ⟨u⟩ and ⟨v⟩; the maximum and minimum velocity dispersions, σ_{max} and σ_{min}; the ratio of the velocity dispersions; and the vertex deviation.

A sample of the results of our simulations is shown in Figure 2 which gives the distribution of the representative points on the velocity plane and the corresponding velocity ellipse. The sample is one of the models of case 7, i.e., for a stellar age of 6.5×10^7 years, with the stars ending up at less than 200 pc from the sun after being born in an arm. The corresponding parameters of the velocity ellipse are:

$$\langle u \rangle = -7.8 \text{ km s}^{-1} \qquad \langle v \rangle = +0.7 \text{ km s}^{-1}$$
$$\sigma_{max} = 9.6 \text{ km s}^{-1} \qquad \sigma_{min} = 5.4 \text{ km s}^{-1}$$
$$l_v = -17.^{\circ}6$$

The departure of the mean values from the origin and the vertex deviation are clearly noticeable in the figure.

IV. DISCUSSION

The smoothing or blurring caused by background stellar field comes out clearly from a comparison of the models that consider only stars nearer than 200 pc from the sun, with those that extend that limit to 400 pc (i.e., models 1 and 2, 3 and 4, 5 and 6, and 7 and 8): within the errors, the larger the region considered, the smaller (in absolute value) the vertex deviation. Other parameters, like mean velocity components, and velocity dispersions and their ratio, remain essentially unaltered when the radius of the solar neighborhood is changed.

Table 2 clearly shows the influence of the stellar age

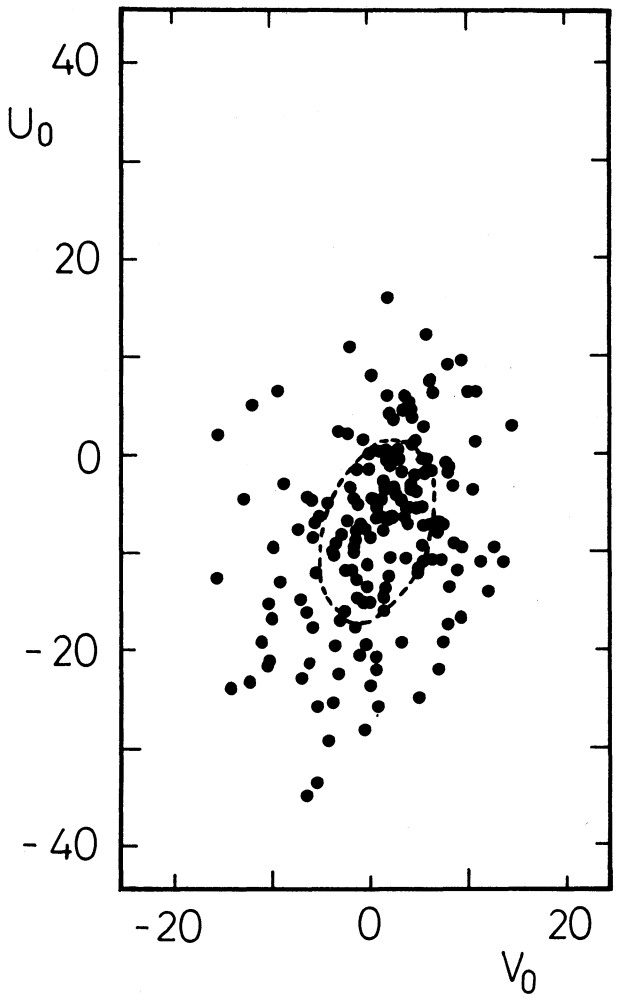

Fig. 2. Representative points on the velocity plane and velocity ellipse for one model of case 7.

on the ratio of velocity dispersions and on the vertex deviation: the older the stars, the smaller ratio of the dispersion and the absolute value of the vertex deviation. The simple picture described in Section II is however modified by the different modelling effects. First, except for the not significant value of model 11, all the vertex deviations are negative, although models 3, 4, 7, 8, 11, 12, 15, 16 and specially, 17 and 18 correspond to ages larger than $\tau = \pi/2\kappa$ (about 5×10^7 years). Also, dispersion ratios as low as $4\ B^2/\kappa^2$ (about 0.40) are never reached either; for $\tau = 6.5 \times 10^7$ years and 13×10^7 years, the dispersion ratios are rather similar to the theoretical steady state value of $[-B/(A - B)]^{1/2} \cong 0.63$.

The main changes take place for ages smaller than 6.5×10^7 years, as the values for 13×10^7 years do not differ appreciably from those for 6.5×10^7 years; notice, however, that the presence of an arm might alter the preceding conclusion about the vertex deviation (models 5, 7 and 18).

The effect of limiting the region of star formation to an "arm" (models 5 through 8 and 18) is very little for the youngest stars; the only difference between models 1 and 2 and models 5 and 6, seems to be that the mean u velocity is not negligible for the latter. For $\tau = 6.5 \times 10^7$ and 13×10^7 years, however, the effect of an arm seems to be an increase of the vertex deviation, in addition to the important mean u and v velocities.

The effect of the systematic initial velocity on the mean velocity is very clear, as had been anticipated in the previous section. For $\tau = 1.8 \times 10^7$ years there is no change in the vertex deviation (model 1 and models 9 and 10); for $\tau = 6.5 \times 10^7$ years, the vertex deviation of model 12 agrees very well with the one of model 3, but the departure of model 11 suggests a real difference.

The superposition of systematic velocity components seems to result in a linear superposition of the mean velocities for each component (compare models 9, 10 and 19, and models 11, 12 and 20) and, again, little or no effect on the velocity dispersions, their ratio and the vertex deviation.

The superposition of an arm with the systematic velocity (models 5, 9 and 13; 5, 10 and 14; 7, 11 and 15; 7, 12 and 16) shows again a linear superposition of the mean velocities for $\tau = 1.8 \times 10^7$ years, but a not so linear superposition for $\tau = 6.5 \times 10^7$ years. There is no apparent effect on the dispersions, but a curious one appears on the vertex deviation: for $\tau = 1.8 \times 10^7$ years there seems to be an addition of effects (models 5, 9 and 13, and models 5, 10 and 14), while for $\tau = 6.5 \times 10^7$ years there seems to be an averaging of effects (models 7, 11 and 15, and models 7, 12 and 16); the errors are very large, however, and it is difficult to establish the true result.

V. CONCLUSION

Assuming that: *a)* stars just born have a circular velocity distribution in the galactic plane, *b)* stellar formation proceeds at a constant rate over a time span similar to the maximum stellar age, and *c)* stellar orbits in the galactic plane are close enough to circles to be adequately represented by the epicyclic approximation, we have shown that both the vertex deviation and the increase with stellar age of the velocity dispersion ratio are direct consequences of the differential stellar motions, at least for stars whose maximum ages do not exceed a few times 10^7 years.

The presence of systematic velocity components when stars are born, or the fact that stars form in spiral arms, does not alter the previous conclusions. For stellar ages of about 10^8 years or larger, those phenomena may have an appreciable effect, however; as they also yield not negligible mean velocities, the observed values of the solar motion pose some limitations to the conditions that can be postulated for just born stars.

For stellar ages of about 10^8 years the ratio of velocity

dispersions and the vertex deviation are close to the theoretical steady state values.

We would like to conclude by noting that our assumption *b)* may be questioned because star formation is not continuous, neither in space nor in time. The same problem is also present in previous attempts to explain the vertex deviation, however, and it emphasizes the difficulty, pointed out in the Introduction, to use the vertex deviation as a check for theories of star formation in spiral arms. Our results show that even under very simple hypotheses the main features of the deviation can be adequately explained.

We are grateful to Mr. G. Ginestet, Mrs. S.D. Abal de Rocha and M.C. Fanjul de Correbo, and Mr. R.C. Leonardi for technical and clerical assistance. The HP 1000 computer used for this investigation was purchased with grants from the Comisión de Investigaciones Científicas de la Provincia de Buenos Aires and from the Secretaría de Estado de Ciencia y Tecnología. The former also contributed with other grants.

REFERENCES

Delhaye, J. 1965, in *Galactic Structure*, eds. A. Blaauw and M. Schmidt, 61.
Filin, A. Ia. 1957, *Astr. Zh.*, **34**, 525.
Hilton, J.L. and Bash, F. 1982, *Ap. J.*, **255**, 217.
Kerr, F.J. 1968, in *Nebulae and Interstellar Matter*, eds. B.M. Middlehurst and L.H. Aller, 575.
Lindblad, B. 1959, *Handbuch der Physik*, (Berlin: Springer-Verlag), LIII, 21.
Nordström, H. 1936, *Meddel. Lund. Ser. II*, No. 79.
Ogorodnikov, K.F. 1965, *Dynamics of Stellar Systems* (New York: Pergamon).
Schmidt, M. 1965, in *Galactic Structure*, eds. A. Blaauw and M. Schmidt, 513.
Woolley, R. 1970, in *IAU Symposium No. 38, The Spiral Structure of our Galaxy*, eds. W. Becker and G. Contopoulos, (Dordrecht: D Reidel), p. 423.
Yuan, C. 1971, *A.J.*, 76, 664.

Lilia P. Bassino, Víctor H. Dessaunet, and Juan C. Muzzio: Observatorio Astronómico de La Plata, Paseo del Bosque s/n, 1900 La Plata, Argentina.

Rev. Mexicana Astron. Astrof., 13, 15-25 (1986)

LOW DENSITY IONIZED GAS ASSOCIATED WITH M17, G333.3 – 0.4 AND RCW 74

I.N. Azcárate[1], J.C. Cersosimo[1], and F.R. Colomb[1]

Instituto Argentino de Radioastronomía
Argentina

Received 1985 August 6

RESUMEN

Se realizaron observaciones en la línea H166α y el continuo a 1.4 GHz en diferentes posiciones en el gas ionizado extendido, asociado a las regiones H II, M17, G333.3 – 0.4, y RCW 74, respectivamente. Se obtuvieron temperaturas electrónicas y otros parámetros físicos de estas regiones y se les comparó con los obtenidos por otros autores a partir de observaciones de líneas de recombinación en radio de más alta frecuencia. Los resultados son compatibles con una descripción de las regiones H II relativamente extendidas, como compuestas por una pequeña región compacta (N_e = 100-1000 cm^{-3}), rodeada de una envoltura de gas ionizado de más baja densidad ($N_e \cong$ 1-10 cm^{-3}). Las temperaturas electrónicas parecen variar con la densidad, al menos en M17.

ABSTRACT

We made observations in the H166α line and in the 1.4 GHz continuum at several positions in extended ionized gas associated with the H II regions M17, G333.3 – 0.4, and RCW 74, respectively. We derived electron temperatures and other physical parameters of these regions and compared them with those obtained by other authors from higher frequency radio recombination line observations. The results are compatible with a description of relatively extended H II regions, each consisting of a small compact region (N_e = 100 to 1000 cm^{-3}) embedded in a extended ionized gas envelope of lower density ($N_e \cong$ 1-10 cm^{-3}). Electron temperatures appear to vary with density, at least in M17.

Key words: INTERSTELLAR MATTER — NEBULAE-H II REGIONS — RADIO RECOMBINATION LINES

I. INTRODUCTION

The H166α line has been observed along the galactic plane for $|l| < 50^\circ$ (Lockman 1976; Hart and Pedlar 1976; Hart *et al.* 1983). This line emission correlates well with the CO emission at 115 GHz, both in distribution and in velocities, (Robinson *et al.* 1984). As is well known, CO is a primary tracer of H_2 in giant molecular clouds. The close association found between giant molecular clouds and H166α emission suggest that this is a good indicator of star formation regions.

The purpose of this paper is to study the H166α emission from the low density and extended ionized gas regions associated with the H II regions M17, G333.3 – 0.4, and RCW 74. To this end we report observations of the three nebulae. M17, G333.3, and RCW 74, have been observed previously at other radio recombination lines, in the radio continuum at different frequencies, in some molecular lines (CO, H_2CO, OH, etc.) as well as at optical wavelengths.

Let us consider first M17. This region has been studied in a large number of radio recombination lines with frequencies ranging from 408 MHz to 88.5 GHz (Goudis 1976), in the optical range and radio lines of CO, H_2CO, OH, H_2O. Molecular line studies of the associated molecular cloud to the small and dense central region have been published by Lada, Dickinson, and Penfield (1974); Lada (1976); Elmegreen and Lada (1976), and Thronson and Lada (1983). H_2O and OH masers toward M17 have been discussed by Knowles, Caswell, and Goss (1976) and Genzel and Downes (1977). H_2CO in absorption was observed by Whiteoak and Gardner (1974), and Downes *et al.* (1980) at velocities (LSR) 23.7 and 23.5 km s^{-1}, respectively (throughout this paper all velocities are referred to the Local Standard of Rest). In CO the velocity is 20 km s^{-1} (Lada *et al.* 1974), and in H_2O it is 19 km s^{-1} (Genzel and Downes 1977). Excited OH emission velocity is 21 km s^{-1}, according to Knowles *et al.* (1976). In general, molecular line velocities agree with recombination line velocities.

The optical observations of [O III] (λ = 5007 A) made by Elliot and Meaburn (1975) show single, double and quadruple profiles, indicating the very complex kinematics of the region, with probably unusual large scale internal motions produced by ionization fronts eating into the adjacent neutral material (Meaburn 1977).

Most of the radio recombination line observations made generally at frequencies $\geqslant$ 5 GHz and with anten-

1. Member of the Carrera del Investigador Científico y Tecnológico del Consejo Nacional de Investigaciones Científicas y Técnicas (*CONICET*), Argentina.

na beams $< 4'$, in the direction of the center of the nebula (G15.0 −0.7), show a single profile. Exceptions are the H76α observations of Gull and Balick (1974) and McGee and Newton (1981), showing double profiles. The H252α observations of Batty (1974), show a difference of 12 km s^{-1} in radial velocities as compared with higher frequency observations.

The region centered at galactic coordinates l = 333.3°, b = −0.4° (we shall call it G333.3) has been observed in H109α, H76α, H90α, and in molecular lines from H_2CO, OH and CO. Observations of CO (J = 1→0) were made by Gillespie *et al.* (1977). The transition CO (J=2→1) has been studied with more detail by De Graauw *et al.* (1981) in the associated molecular cloud. H_2CO was observed in absorption by Whiteoak and Gardner (1974). Molecular line velocities are in general $\simeq -51$ km s^{-1}, in good agreement with recombination line-velocities.

RCW 74 (G305+4, 0.2) has been observed in the H109α, H76α, H252α lines, CO (Gillespie *et al.* 1977; Brand *et al.* 1984), H_2CO (Whiteoak and Gardner 1974), and OH. Molecular line velocities fall in the range −35 km s^{-1} to −40 km s^{-1}. Recombination line velocities are $\simeq -40$ km s^{-1}.

We shall describe in the next section observation carried out of the H166α line and 1.4 GHz continuum, which seem to prove the existence of extended emission regions embedding the three nebulae.

II. OBSERVATIONS

a) *The Line*

The observations were made with the 30-meter diameter antenna of the Instituto Argentino de Radioastronomía. The noise temperature of the system was about 85 K for a cold sky background and the half-power beam-width (HPBW) was 34 arcmin at 1420 MHz. The frequency-switching technique was used for the observations. The back-end included a filter bank of 112 filters of 10 kHz widths. These gave a velocity resolution of 2 km s^{-1}. We observed 9 positions for each H II region, at a separation of 0.5°. The total integration time was about four hours for each position. This resulted in an 'rms' noise of 0.025 K. The final profiles were obtained by removing the instrumental baselines using in most of the cases a second order polynomial.

b) *The Continuum*

The three nebulae were observed in the continuum at 1420 MHz by making several right ascension scans spaced 0.5° in declination. The continuum receiver covered a bandwidth of 40 MHz centered at 1420 MHz. A filter of 2MHz bandwidth centered at 1420.4057 MHz was used to eliminate the emission from galactic neutral hydrogen. The receiver was operated in the Dicke switching mode. The velocity of the right ascension scans was 0.5° minute.

III. RESULTS

a) *Structure of M17*

The galactic coordinates and some parameters of the observed profiles are given in Table 1. Some of the profiles are shown in Figure 1. The central profile, as well as several other ones, have centroid velocities of 20 km s^{-1}. Other profiles, as the one at l = 14.5°, b = 0.0°, have centroid velocities of 35 km s^{-1}. This would mean that emission has originated (for that profile, according to the Schmidt rotation model), from more distant regions along the line of sight. The FWHM (Full-Width-Half-Maximum) is 35 km s^{-1} for most of the profiles.

TABLE 1

PARAMETERS CALCULATED FOR DIFFERENT OBSERVED POINTS IN M17

l (°)	b (°)	$\int T_L\,dv$ (K km s^{-1})	T_c (K)	T_e^* (K)
14.5	0.0	7.364	8	3251 ± 300
14.5	− 0.5	3.092	8	6900 ± 700
15.5	0.0	0.578	8	–
14.5	− 1.0	1.792	14	–
15.5	− 1.0	4.856	11.6	6450 ± 650
15.5	− 0.5	5.108	20	10000 ± 100
15.0	− 1.0	11.140	26	6300 ± 600
15.0	− 0.7	25.453	38	4300 ± 400
15.0	0.0	2.204	4	5000 ± 500

The continuum map of the observed region is shown in Figure 2. The numbers at the contour levels correspond to degrees Kelvin of antenna temperature. The positions given in Table 1 are shown by X marks. The values of the continuum antenna temperatures T_c, given in the map and the integrated power $\int T_L\,dv$ under the corresponding H166α profiles, were used to derive electron temperatures T_e (cf. Table 1). The values of T_e obtained in this way range from 3000 to 12000 K.

The integrated flux density from the region associated with M17 is 675 Jy. Using this value and according to a very simplified model of a spherical H II region with uniform electron temperature and density given by Schraml and Mezger (1969), we computed an rms electron density $\cong 12$ cm^{-3} and obtained a value of emission measure of 1.04×10^4 pc cm^{-6}. The adopted distance is 2.3 kpc and the diameter of the spherical model is D ≅ 50 pc.

Higher frequency observations in the direction of G15.0, −0.7, which is the center of the observed region (Wilson *et al.* 1970; McGee and Newton 1981; Downes *et al.* 1980) show density and emission measure values about two orders of magnitude greater than our values (see Table 2). This difference can be explained by the

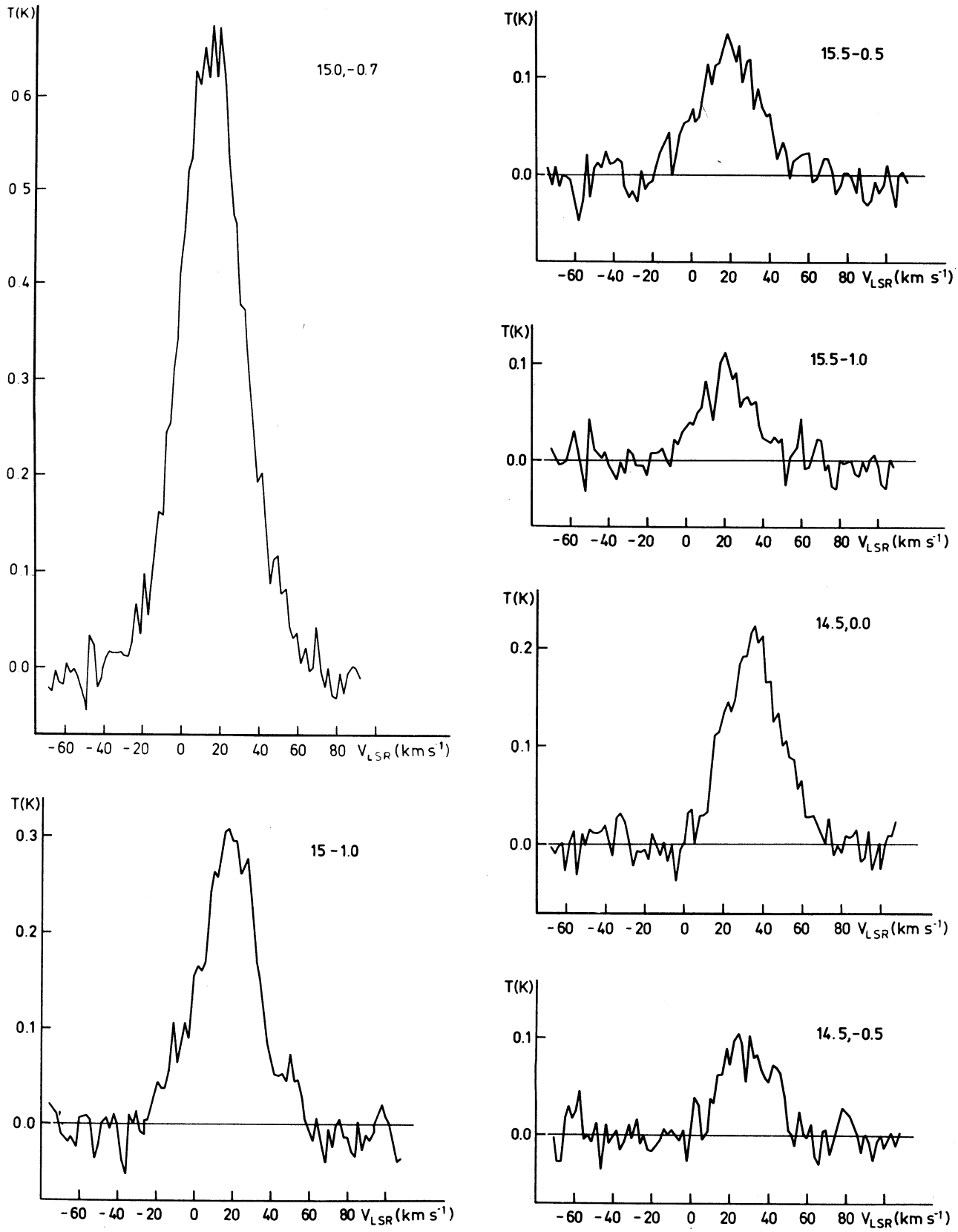

Fig. 1. Some profiles obtained from the H166α observations of the M17 region.

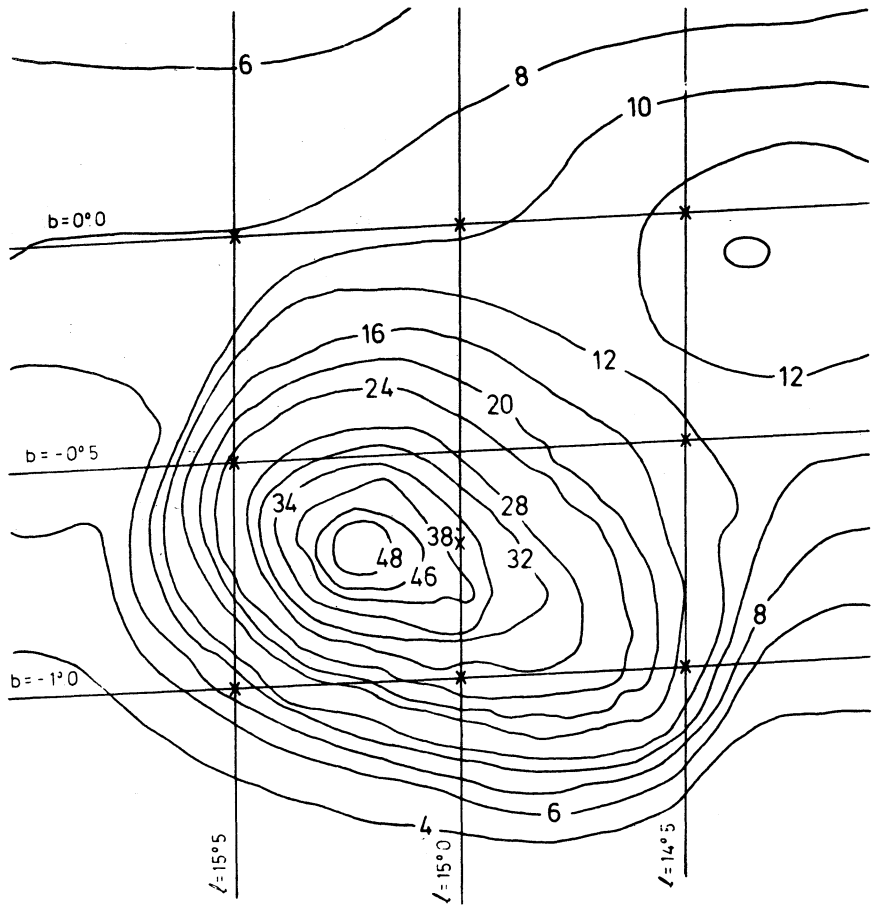

Fig. 2. Continuum map at 1420 MHz of the region associated with M17. The crosses indicate the positions where the H166α observations were made.

TABLE 2

PHYSICAL PARAMETERS OBTAINED FROM DIFFERENT RECOMBINATION LINE OBSERVATIONS FOR M17, G333.3 AND RCW 74

	M17			G333.3			RCW 14		
Reference	EM (pc cm^{-6})	N_e (cm^{-3})	T_e (K)	EM (pc cm^{-6})	N_e (cm^{-3})	T_e (K)	EM (pc cm^{-6})	N_e (cm^{-3})	T_e (K)
Wilson *et al* (1970) H109α	1.6×10^6	594	6200	2.1×10^6	994	5000	5.1×10^5	223	5200
Downes *et al* (1980) H110α	1.6×10^6	–	9100	–	–	–	–	–	–
McGee and Newton (1981) H76α	3×10^6	1010	8300	7.5×10^5	456	7400	7.2×10^5	456	6900
Our observations (1984) H166α	1.04×10^4	12	5500	8.5×10^3	7	5200	8.81×10^3	5	4500

fact that at the frequency of the H166α line and with our antenna beam, the observations are most sensitive to the extended and diffuse parts of the nebula, the compact and higher emission measure regions near the center becoming optically thick at 1.4 GHz and suffering greater beam dilution.

b) *Electron Temperatures*

The electron temperatures were derived from the observed H166α profiles by using the line to continuum ratio technique. The formula used was:

$$\frac{\int T_L\, dv}{T_c} = \frac{7440}{a(\nu, T_e)} \frac{1}{1+(N(He^+)/N(H^+))} \times \left(\frac{\nu}{GHz}\right)^{1.1} \left(\frac{T_e^*}{K}\right)^{-1.15} \quad (1)$$

where T_e^* is the electron temperature if the emission levels are in Local Thermodynamical Equilibrium (LTE), $a(\nu, T_e)$ is a factor close to unity, tabulated by Mezger and Henderson (1967), ν is the line frequency in GHz, $N(He^+)/N(H^+)$ is the number density ratio of ionized helium to ionized hydrogen generally assumed to be 0.1, $\int T_L\, dv$ is the integral power under the line (in K km s^{-1}) and T_c is the continuum antenna temperature.

If it is assumed that T_e is constant over the whole region, then $\int T_L\, dv$ should be proportional to T_c. In Figure 3, we have plotted $\int T_L\, dv$ against T_c. A least squares straight-line fit to the observed points, excluding those corresponding to $\ell = 14.5°$, $b = -1.0°$, $\ell = 15.5°$, $b = 0.0°$ (very noisy profiles), results in a slope which corresponds to $T_e = 4800 \pm 480$ K. This method has been used by other authors (Jackson and Kerr 1975; Hart and Pedlar 1976) to estimate the electron temperature in the presence of non-thermal continuum uniformly distributed over the whole source. The electron temperature computed in this way, is independent of the non-thermal continuum emission. This should be the case with the general non-thermal galactic continuum emission.

By looking at Figure 3, it can be seen that the fitting by a straight line is not very satisfactory, in particular for the data corresponding to the position of galactic coordinates $\ell = 15.5°$, $b = -0.5°$ ($\int T_L\, dv = 5.108$ K km s^{-1}, $T_c = 20$ K). That would indicate that the non-thermal contribution in that direction is greater than at the other points, that is to say there would be contributions to the continuum along this particular line of sight, from regions without H166α emission. However, the correlation coefficient (0.8934), estimated by using the 't' Student distribution (Moroney 1951), suggests that the correlation is significant.

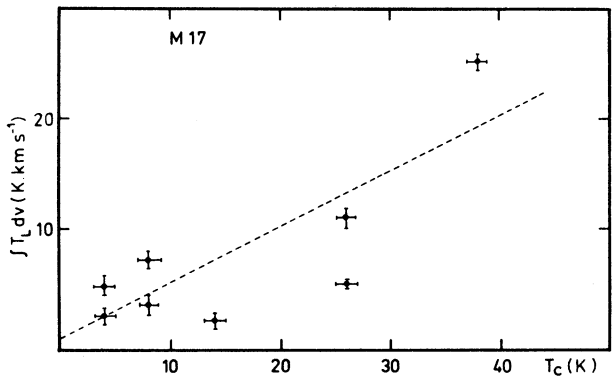

Fig. 3. $\int T_L\, dv$ versus T_c for M17. The dashed line corresponds to the least squares straight-line fit to the observational results.

On the other hand, the mean value of T_e^* obtained from the individual profiles, excluding the position at $\ell = 15.5°$, $b = -0.5°$ (cf. Table 1) is $T_e^* = 5400$ K. This value is not very different from the one obtained by means of the statistical method considered above. Therefore, we can assume that an average value of 5000 K as a first approximation is a good estimate for the electron temperature of the low density ionized gas ($N_e \simeq 12$ cm^{-3}) associated with M17.

b) *G333.3*

The galactic coordinates and other parameters of the observed profiles are shown in Table 3. Some of the profiles are shown in Figure 4. The centroid velocities of the profiles are $\simeq -50$ km s^{-1}, having a FWHM of 30 km s^{-1}. The asymmetry of some profiles, given by the possible presence of a component at more negative velocities, could be due to ionized gas at a larger distance than the H II region we are studying.

TABLE 3

PARAMETERS CALCULATED FOR DIFFERENT OBSERVED POINTS IN G333.3

ℓ (°)	b (°)	$\int T_L\, dv$ (K km s^{-1})	T_c (K)	T_e^* (K)
333.3	− 0.4	12.18	26	5800 ± 600
334.0	− 0.5	1.722	8	1000 ± 1000
334.0	0.0	2.718	10	9400 ± 900
333.5	0.0	5.860	14	6450 ± 650
334.0	− 1.0	1.354	4	7760 ± 800
333.0	− 1.0	2. 714	10	9400 ± 900
333.5	− 1.0	1.818	5	7290 ± 700
333.0	0.0	5.426	12	6000 ± 600
333.0	− 0.5	12.88	26	5600 ± 500

The continuum map is shown in Figure 5. The positions where the line was observed are shown by crosses. The values of electron temperatures for each position are given in Table 3 and range from 6000 to 11000 K. The integrated flux density for the extended region associated to G333.3 of about 2° of diameter is 1500 Jy. Under the same simplified assumptions made for M17 (uniform electron temperature and density) we computed a rms electron density $\simeq 7$ cm^{-3} and a value for the emission measure of 8.10^3 pc cm^{-6}. The adopted distance is 3.9 kpc and the diameter of the spherical model is $D \simeq 129$ pc.

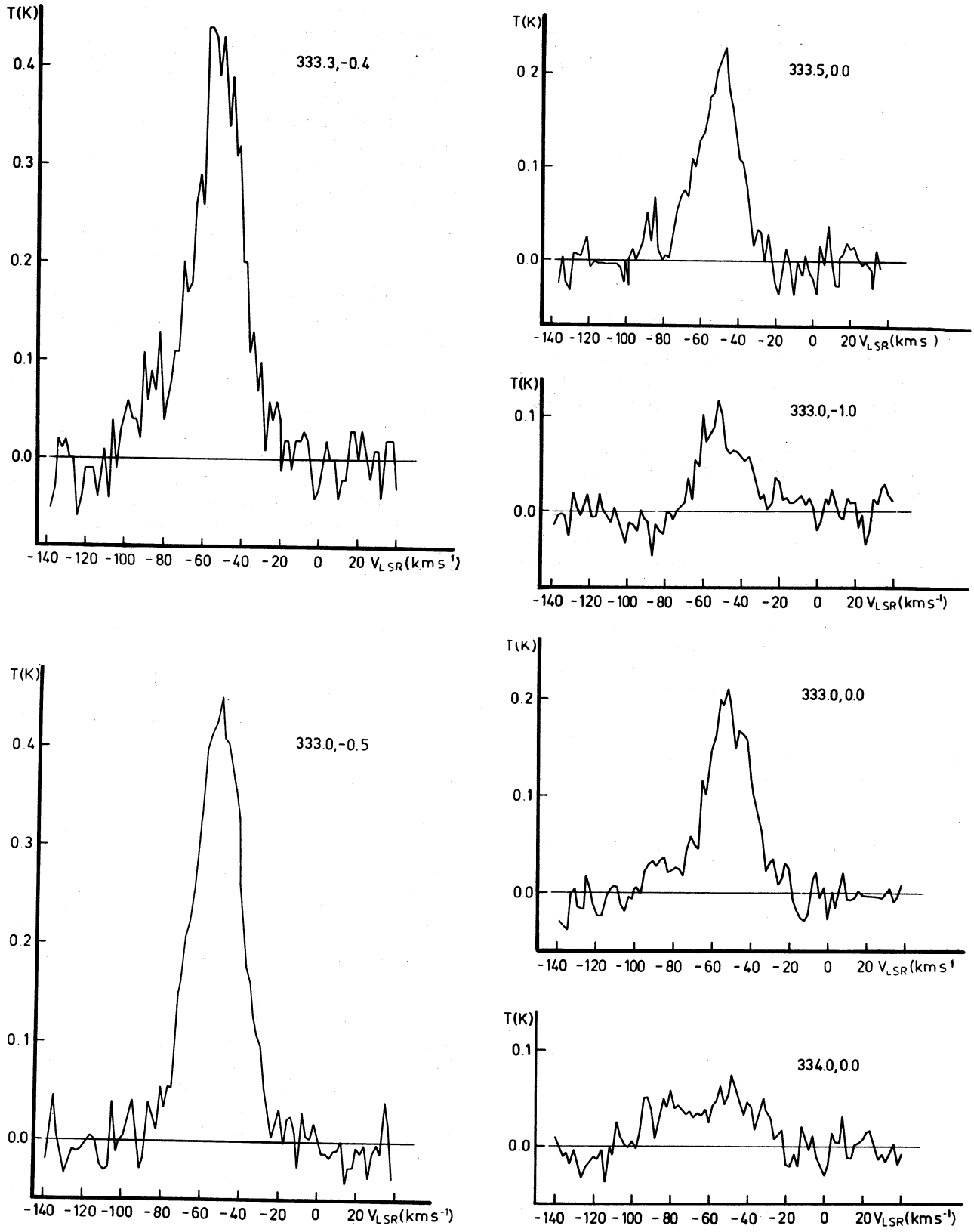

Fig. 4. Some profiles obtained from the H166α observations of the G333.3 region.

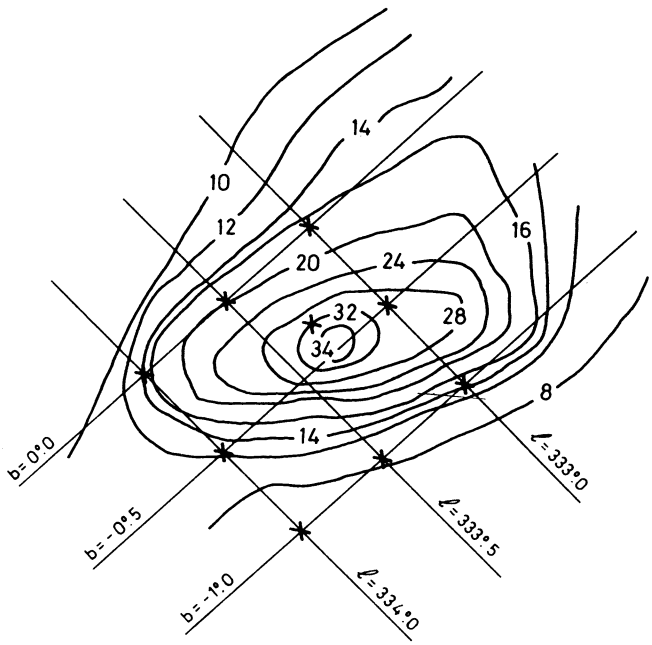

Fig. 5. Continuum map at 1420 MHz of the region associated to G333.3 The crosses indicate the positions where the H166α observations were made.

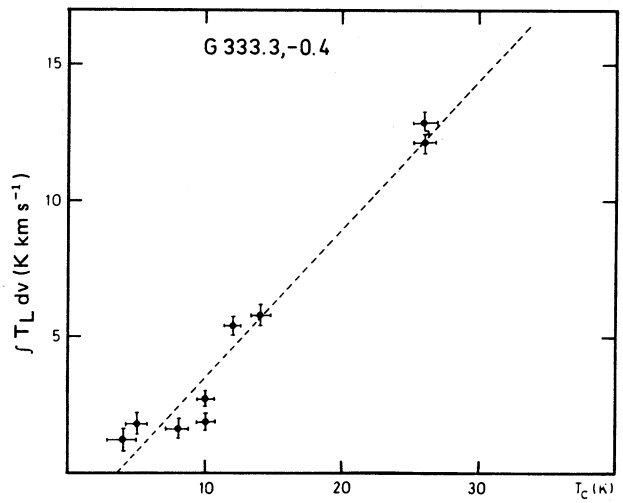

Fig. 6. $\int T_L$ dv versus T_c for G333.3. The dashed line corresponds to the least squares straight-line fit to the observational results.

As in the case of M17, higher frequency radio recombination line observations in the direction of G333.3, −0.4 (the center of the HII region), (Wilson *et al.* 1970; McGee and Newton 1981) result in values of density and emission measure one or two orders of magnitude larger than those obtained from our measurements (see Table 2). This fact can be explained by the same argument given for M17.

By means of the statistical method referred to above, we estimated an average value for the electron temperature of the low-density ionized gas associated to G333.3 of 5200±500 K. We show in Figure 6 $\int T_L$ dv versus T_c and the corresponsing straight-line fit.

c) *RCW 74*

Galactic coordinates and other parameters of the observed profiles are shown in Table 4. Some of the profiles are shown in Figure 7. The centroid velocities of most of the profiles are $\simeq -40$ km s^{-1}, with FWHM of $\simeq 35$ km s^{-1}.

We shown the continuum map in Figure 8. We have indicated with X marks the positions where the H166α line was observed. The values of the computed electron temperatures are given in Table 4, ranging from 4500 to 7500 K. The integrated flux density for the extended region associated to RCW 74 of about 110 arcmin diameter is 1400 Jy. Using the formulation of Schraml and Mezger (1969) the obtained values of electron density and emission measure are $\simeq 7$ cm^{-3} and 8.77×10^3 pc cm^{-6}, respectively. The adopted distance is 3.4 kpc and the diameter of the source is $\simeq 112$ pc.

TABLE 4

PARAMETERS CALCULATED FOR DIFFERENT OBSERVED POINTS IN RCW 74

ℓ (°)	b (°)	$\int T_L$ dv (K km s^{-1})	T_c (K)	T_e^* (K)
305.0	− 0.5	2.140	6	7400 ± 700
305.0	+ 0.5	3.660	6	4650 ± 450
306.0	0.0	2.420	5	5650 ± 600
305.5	+ 0.5	4.040	8	5481 ± 5500
305.4	+ 0.2	13.00	22	4780 ± 500
305.0	0.0	7.30	12	4660 ± 450
306.0	− 0.5	1.646	3	5100 ± 500
306.0	+ 0.5	0.432	3	–
305.5	− 0.5	2.838	8	7450 ± 750

Again our values of electron density and emission measure are lower than those obtained from H109α line observations by Wilson *et al.* (1970) and H76α ones by McGee and Newton (1981) (cf. Table 2). The same explanation of this difference as given for M17 and G333.3, should also be valid here. By means of the same method we used for M17 and G333.3, we derive an average electron temperature of 4500±450 K for the low density ionized gas associated to RCW 74. The plot of $\int T_L$ dv versus T_c is shown in Figure 9, together with the corresponding fitted straight-line.

IV. THERMODYNAMICAL EQUILIBRIUM

In the high emission measure regions, there are important departures from LTE at the frequency of 1.4 GHz. This results in an increment of the recombination

line temperatures, and therefore generally there is an underestimation of the T_e (LTE). For the low density ionized gas ($N_e \cong 1-10\ cm^{-3}$), of lower emission measure, the T_e^* obtained from H166α and 1.4 GHz continuum observations, should differ from the actual temperature by less than 20% (Dyson 1969). On the other hand, Shaver (1980), shows that, for a given emission meas-

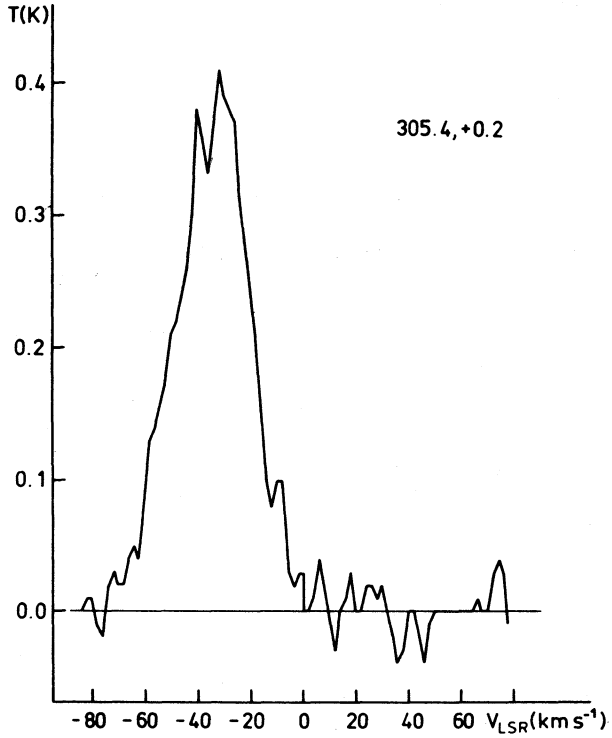

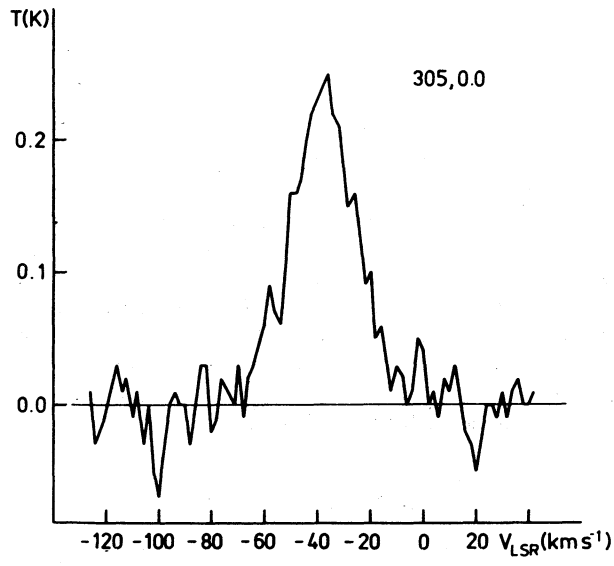

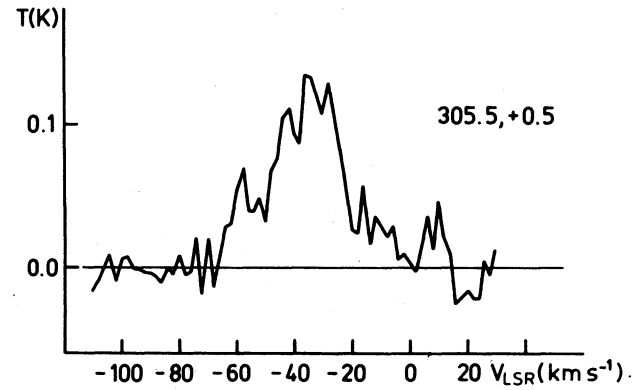

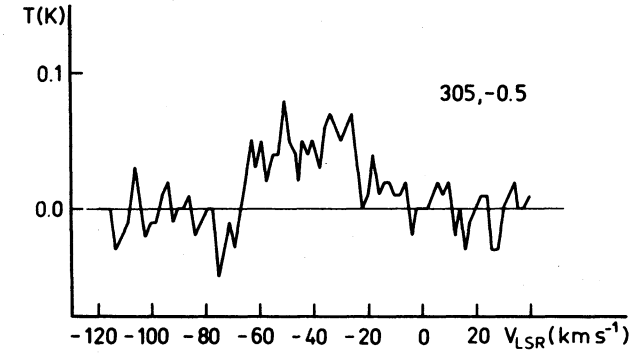

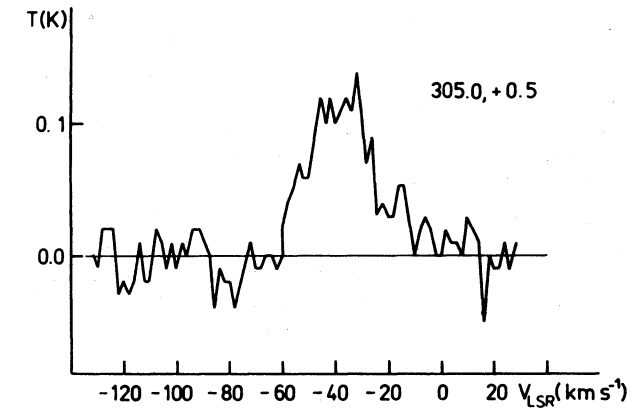

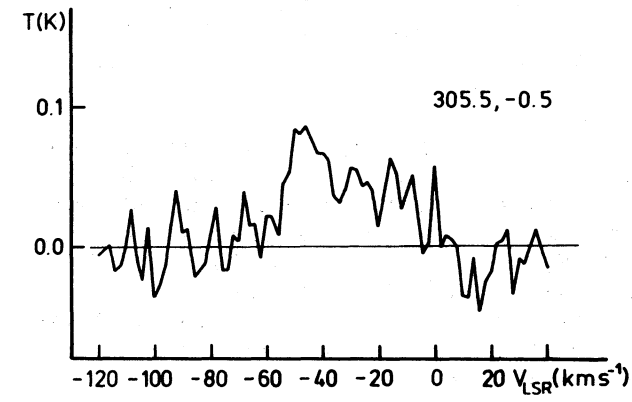

Fig. 7. Some profiles obtained from the H166α observations of the RCW 74 region.

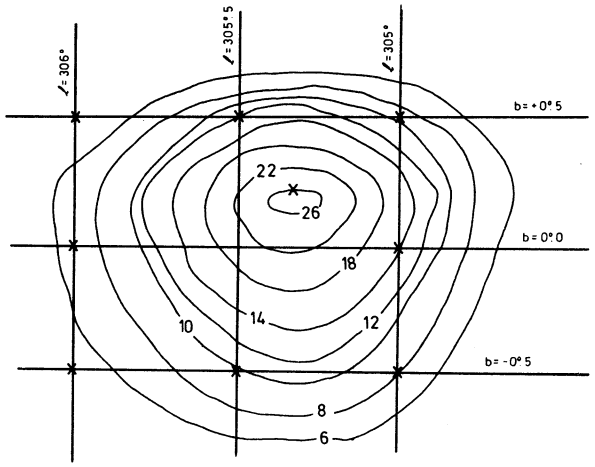

Fig. 8. Continuum map at 1420 MHz of the region associated to RCW 74. The crosses indicate the positions where the H166α line observations were made.

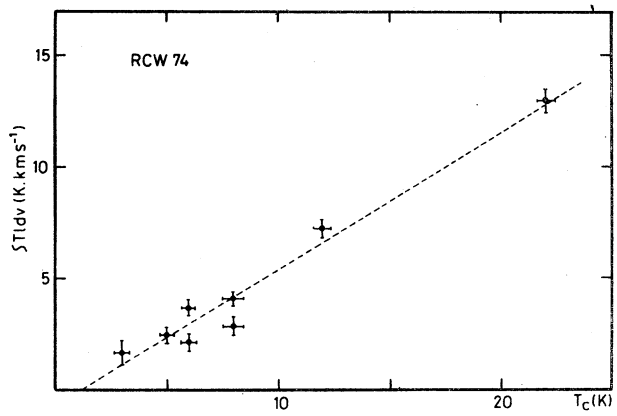

Fig. 9. $\int T_L$ dv versus T_C for RCW 74. The dashed line corresponds to the least squares straight-line fit to the observational results.

ure, there is a unique frequency at which $T_e = T_e^*$. It turns out from his results that at 1.4 GHz and for E.M. = $10^3 - 10^4$ pc cm^{-6}, $T_e \simeq T_e^*$.

In the three regions we observed, the possibility that departures from LTE are present, was investigated through the expression for the ratio of the actual electron temperature T_e, to the value T_e^* obtained by assuming LTE:

$$\frac{T_e}{T_e^*} = \left[b_n \left(1 + \frac{\tau_c}{2} \frac{k T_e}{h\nu} \frac{d \varrho_n b_n}{d b_n} \Delta_n \right) \right]^{0.87} \qquad (2)$$

where τ_c is the optical depth for the continuum radiation, b_n is the population departure for the atomic level n. Using the coefficients given by Brocklehurst (1970), we obtained values of $T_e/T_e^* \leqslant 1.2$ for the three regions, as expected.

These results can be explained in two ways either: *i*) there is a compensation between stimulated emission in the low density outer regions by the continuum radiation of the inner core regions and pressure broadening which may be present in the nebulae, or *ii*) the effects of departure from LTE are negligible in our observations and furthermore, pressure broadening is not significant. The latter alternative seems more likely. Pressure broadening does not play a dominant role because the $\Delta\nu_S/\Delta\nu_D$ ratio (Griem 1967) is unimportant for $n > 150$ when the density is $N_e \leqslant 10^3$ cm^{-3}; $\Delta\nu_S$ is the Stark (electron collision) broadened line half-power width, and $\Delta\nu_D$ is the Doppler half-power width.

Therefore, we conclude that the assumption of LTE is a good approximation for the low density gas associated with the three regions.

V. ELECTRON TEMPERATURE VARIATION ACROSS THE H II REGIONS

In Figure 10 we show different electron temperature values obtained for M17, from several radio recombination line observations with different beam sizes (HPBW), as taken from the review by Goudis (1976) as well as from other references (Pedlar and Davies 1972; McGee and Newton 1981; Downes *et al.* 1980; McGee *et al.* 1975). We also include our result (T_e = 5000 K, with a HPBW of 34′). It can be seen from the figure that the temperatures range from 8000 to 4500 K, showing a general trend of decrement as the HPBW increases. In addition, smaller beams correspond generally to higher frequency observations. Two effects ensure that low frequency spectra ($\nu \leqslant 1.4$ GHz) will largely reflect conditions in low-density gas. One of them is the optical

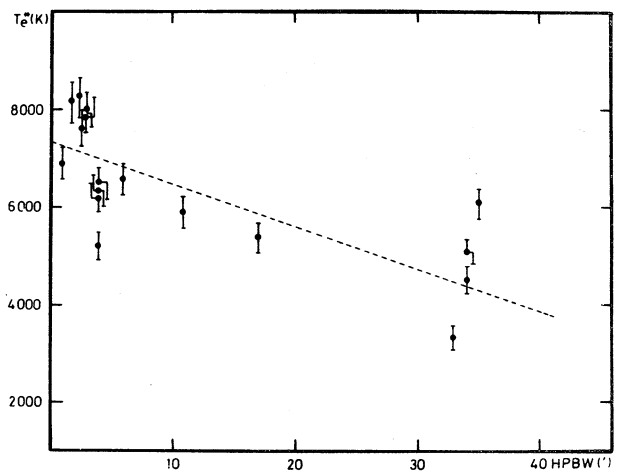

Fig. 10. Plot of electron temperature T_e against beam sizes (HPBW), as obtained from various radio recombination line observations of M17. The dashed line corresponds to the least squares straight-line fit to the observational results.

depth in the continuum for ionized gas, which at the frequency of 1.4 GHz is greater than unity when the emission measure is $> 10^6$ pc cm^{-6}. The second effect arises from impact broadening of the line in dense regions. At 1.4 GHz this broadening will significantly decrease peak line temperatures when $N_e > 1000$ cm^{-3} (Lockman 1976). At high frequencies ($\nu \geqslant 5$ GHz) the observed spectra will be dominated by regions of high N_e, that is to say it will reflect conditions of denser gas.

Therefore, the presence of a variation of the electron temperature with the density in the nebula is apparent. This effect (decreasing electron temperature with decreasing density) has been considered by Pedlar (1980), and Garay and Rodríguez (1983) by comparing electron temperatures of low density and high density H II regions. Low density H II regions are in general cooler than high density ones, due to the lack of collisional de-excitation, that inhibits cooling. In our analysis, we considered the temperature variation across the same region. In this case, there are no effects due to the galactic temperature gradient with the galactocentric distance. Therefore, a model of a hot and high density central region and a low density and cooler envelope, is suitable for describing at least M17.

VI. STAR FORMATION

Compact H II regions expand, and, as their size increases their density and central emission measure decreases. Expansion of the H II regions continues, until they achieve pressure equilibrium with the surrounding neutral gas, or until the ionizing O stars move off the main sequence. Once the electron densities have decreased to some 10 cm^{-3}, they form extended low density H II regions, with low surface brightness, which are difficult to observe at high radio frequencies. However, the free-free emission from a diffuse region, is easily observable with low angular resolution at decimeter wavelengths. The Lyman photon flux required to maintain the radio H II region is provided by O stars. For determining N_c, the Lyman photon production rate in the H II region, we make use of the measured radio flux density S_ν of the free-free emission and of the known distance. The relation between radio luminosity and N_c (Mezger, Smith, and Churchwell 1974) is given by the equation:

$$N_c = 4.76 \times 10^{48} \left(\frac{T_e}{K}\right)^{-0.45} \left(\frac{S_\nu}{Jy}\right) \times \times \left(\frac{\nu}{GHz}\right)^{-0.1} \left(\frac{r}{kpc}\right)^2 \qquad (3)$$

where T_e is the electron temperature, ν is the frequency in GHz, S_ν is the flux in Jy and r is the distance in kpc. We assume the He/H abundance is zero. The results are shown in Table 5.

TABLE 5

THE THREE OBSERVED REGIONS, TOGETHER WITH THEIR FLUXES AND THE CORRESPONDING VALUES OF LYMAN PHOTON FLUX

Region	Distance from the Sun (kpc)	S_ν (Jy)	N_c (Low Density) (ph s^{-1})	N_c (High Density) (ph s^{-1})
M 17	2.3	675	3.7×10^{50}	5.4×10^{50}
G333.3	3.9	1500	2.3×10^{51}	6.3×10^{50}
RCW 74	3.4	1400	1.8×10^{51}	1.4×10^{51}

Since the lifetime of the H II region is relatively short (Osterbrock 1974), we can assume that the stars are on the Zero Age Main Sequence (ZAMS) and with their spectral types according to some initial mass function. Identifying mass with photon flux by using the total luminosity of ZAMS stellar models and the relation of Panagia (1973), between N_c and luminosity, we may calculate the total mass of ZAMS stars associated with a certain Lyman flux.

In each region, we have two different star formation scenarios, one being earlier (high density gas) than the other one (low density gas). We calculated the Lyman flux for the three regions using the parameters obtained from our observations (see Table 5). Comparing these fluxes with those obtained from high frequency determinations (Smith, Bierman, and Mezger 1978), there are no significant differences. That implies the presence of about the same masses of ZAMS stars ionizing both the low and high density gas. Alternatively, it is conceivable that the ionizing cluster is one and the surrounding gas was already in a core-halo distribution. That would be another possibility, different from the assumption of two distinct star formation scenarios.

VII. COMMENTS

We have observed extensively the three H II regions M17, G333.3 and RCW74, in the H166α line and 1.4 GHz continuum. From the observations we derived physical parameters (electron temperature, density and emission measure) corresponding to the low density ionized gas associated to the regions (as was explained above).

On the other hand, from Table 2, it becomes evident that the observations of the higher frequency radio recombination lines, carried out with smaller beams by other authors, supply the physical parameters (essentially electron density and emission measure), corresponding to the denser gas near the center of the nebula. The combined results (at high and low frequencies) are compatible with the description of the relatively extended H II regions as consisting roughly of a small compact region of gas embedded in an extended ionized gas envelope of lower density, as shown in previous papers (Cersosimo 1982; Cersosimo, Azcárate, and Colomb

1984) and studied in more detail for the 30 Doradus nebula (Cersosimo and Loiseau 1984). The conclusion is that observations at a low frequency, such as H166α line, are suitable for obtaining the physical parameters of the lower density ionized gas.

In addition, we have found an electron temperature gradient across M17, which we consider as being due to the variation of temperature with electron density (Pedlar 1980). The values of the electron temperature which we have obtained for the three regions ($\simeq$ 5000 K) are characteristic of low density ionized gas (Pedlar 1980; Cersosimo *et al.* 1984).

We wish to thank the technical staff of the Instituto Argentino de Radioastronomía. We are grateful to Dr. W.G.L. Poppel for his critical reading and useful discussion of the paper. We also thank Mrs. M. Trotz for making the drawings and Miss P. Hurrell for typewriting the tables. We thank the referee for his useful suggestions to improve the paper.

REFERENCES

Brocklehurst, M. 1970, *M.N.R.A.S.*, **157**, 179.
Brand, J. *et al.* 1984, *Astr. and Ap.*, **139**, 181.
Batty, M.J. 1974, *M.N.R.A.S.*, **168**, 37P.
Cersosimo, J.C. 1982, *Ap. (Letters)*, **22**, 157.
Cersosimo, J.C., Azcárate, I.N., and Colomb, F.R. 1984, *Ap. (Letters)*, **24**, 1.
Cersosimo, J.C. and Loiseau, N. 1984, *Astr. and Ap.*, **133**, 93.
De Graauw, T. *et al.* 1981, *Astr. and Ap.*, **102**, 257.
Downes, D., Wilson, T.L., Bieging, J., and Wink, J. 1980, *Astr. and Ap. Suppl.*, **40**, 379.
Dyson, J.E. 1969, *Ap. and Space Sci.*, 4, 401.
Elliot, K.J. and Meaburn, J. 1975, *Ap. and Space Sci.*, **35**, 81.
Elmegreen, B.G. and Lada, C.J. 1976, *A.J.*, **81**, 1089.
Garay, G. and Rodríguez, L.F. 1983, *A.J.*, **226**, 263.
Genzel, R. and Downes, D. 1977, *Astr. and Ap. Suppl.*, **30**, 145.
Gillespie, A.R. *et al.* 1977, *Astr. and Ap.*, **60**, 221.
Goudis, C. 1976, *Ap. and Space Sci.*, **39**, 273.
Griem, H.R. 1967, *Ap. J.*, **148**, 157.
Gull, T.R. and Balick, B. 1974, *Ap. J.*, **192**, 63.
Hart, L. and Pedlar, A. 1976, *M.N.R.A.S.*, **176**, 135.
Hart, L. Azcárate, I.N., Cersosimo, J.C., and Colomb, F.R. 1983, in *Surveys of the Southern Galaxy*, eds. W.B. Burton and F.P. Israel, D. Reidel Publishing Co., p. 43.
Jackson, P.D. and Kerr, F.J. 1975, *Ap. J.*, **166**, 723.
Knowles, S.H., Caswell, J.L., and Goss, W.M. 1976, *M.N.R.A.S.*, **175**, 537.
Lada, C.J., Dickinson, D.F., and Penfield, H. 1974, *Ap. J. (Letters)*, **189**, L35.
Lada, C.J. 1976, *Ap. J. Suppl.*, **32**, 603.
Lockman, F.J. 1976, *Ap. J.*, **209**, 429.
McGee, R.X. and Newton, L.M. 1981, *M.N.R.A.S.*, **196**, 889.
Meaburn, J. 1977, in *Topics in Interstellar Matter*, ed. H. van Woerden, D. Reidel Publishing Co., p. 81.
Mezger, P.G. and Henderson, A.P. 1967, *Ap. J.*, **147**, 471.
Mezger, P.G., Smith, L.F., and Churchwell, E. 1974, *Astr. and Ap.*, **32**, 269.
Moroney, M.J. 1951, *Facts from Figures*, (London: Penguin Books), p. 135.
Panagia, N. 1973, *A.J.*, **78**, 229.
Pedlar, A. 1980, *M.N.R.A.S.*, **192**, 179.
Pedlar, A. and Davis, R.D. 1972, *M.N.R.A.S.*, **159**. 129.
Osterbrock, D.E. 1974, in *Astrophysics of Gaseous Nebula*, (San Francisco: Freeman and Co.), p. 210.
Robinson, B.J. *et al.* 1984, *Ap. J. (Letters)*, **283**, L31.
Schraml, J. and Mezger, P.G. 1969, *Ap. J.*, **156**, 269.
Shaver, P. 1980, *Astr. and Ap.*, **91**, 279.
Smith, L.F., Bierman, P., and Mezger, P.G. 1978, *Astr. and Ap.*, **66**, 65.
Thronson, H.A., Jr. and Lada, C.J. 1983, *Ap. J.*, **269**, 175.
Whiteoak, J.B. and Gardner, F.F. 1974, *Astr. and Ap.*, **37**, 389.
Wilson, T.L., Mezger, P.G., Gardner, F.F., and Milne, D.K. 1970, *Astr. and Ap.*, **6**, 364.

I.N. Azcárate, J.C. Cersosimo, and F.R. Colomb: Instituto Argentino de Radioastronomía, Casilla de Correos No. 5, Villa Elisa, 1894 Argentina.

Rev. Mexicana Astron. Astrof., 13, 27-32 (1986)

THE BROAD BALMER PROFILES FROM η CARINAE SCATTERED BY DUST OVER THE CAR II REGION

J.A. López

Instituto de Astronomía
Universidad Nacional Autónoma de México

and

J. Meaburn

Department of Astronomy, University of Manchester

Received 1985 August 13

RESUMEN

Se muestra que los perfiles anchos de Balmer ($\sim$ 650 km s^{-1} FWHM) presentes en la región Car II se originan en la emisión de Balmer de η Car, la cual es dispersada por polvo en la región, como fué sugerido por López y Meaburn (1984*b*). Los perfiles de Hα provenientes de η Car que son dispersados por el polvo interestelar han sido detectados hasta 6 minutos de arco alejados de η Car. Si η Car y la filamentosa región Car II están efectivamente localizados a la misma distancia de 2.7 kpc que generalmente se supone para el complejo de regiones H II y cúmulos abiertos de Carina, entonces las componentes están siendo detectadas tan lejos como 5 pc de η Car. Se describe un método directo para fijar el límite inferior de la distancia de η Car. Este se basa en la variabilidad del perfil Hα de η Car y su reflexión retardada sobre la región Car II. Si la distancia de 2.7 kpc es adecuada entonces la reflexión de la última variación conocida del perfil Hα de η Car debe ser vista sobre Car II para finales de 1986.

ABSTRACT

The broad Balmer profiles ($\sim$ 650 km s^{-1} FWHM) present over the face of the Car II region are shown to have their origin in the dust scattered Balmer emission from η Car, as suggested by López and Meaburn (1984*b*). The scattered Hα profiles from η Car have been traced as far as 6 arcmin away from η Car. If η Car and the filamentary Car II region are indeed located at the same distance as the ordinarily assumed one of 2.7 kpc for the H II region/open clusters complex of Carina then the scattered components are being detectable as far as $\sim$ 5 pc away from η Car. A direct method to set a lower limit for the distance to η Car is described on the basis of the variability of the Hα profile of η Car and its retarded reflection on the Car II region. If a distance of 2.7 kpc is adequate, then the retarded reflection of the last known variation of the Hα profile from η Car should be seen on Car II by late 1986.

Key words: NEBULAE — SCATTERING

I. INTRODUCTION

High velocity components present only in the Balmer (Hα and Hβ) lines in the Car II region were reported by Elliot (1979). Given the available information on the region at the time he suggested a supernova origin for these profiles. López and Meaburn (1984*a*, hereafter Paper I) mapped the region at intermediate and low dispersion to investigate the spatial extent of these profiles and any observational evidence for their suggested origin. They concluded that a supernova event was most unlikely to have occurred in the region. However, they did confirm the presence of the high velocity components (up to $\sim$ 1000 km s^{-1}) in the Hα and Hβ lines, and showed that these profiles were present over practically the whole face of the filamentary Car II region. Several alternative possibilities that could account for the observed Balmer profiles, based mainly on collimated flows driven by stellar winds from the very massive stars that surround the area, were discussed in Paper I. A dust scattering mechanism for the origin of the broad profiles was not considered in Paper I since the structure of the Balmer profiles do vary from one position to another (see Figures 4*a* and 4*b* in Paper I and Figure 1 in Elliot 1979).

Almost simultaneously with publication of Paper I, Ruiz, Melnick, and Ortiz (1984) presented new evidence showing that the Hα profile from η Car had varied on a time scale of $\sim$ 1 year. López and Meaburn (1984*b*, hereafter Paper II) compared the spectral characteristics of the Hα and Hβ emission from η Car with those ob-

served over the face of Car II and concluded that given the great similarity among the profiles and the now proven short term variability of the Balmer emission from η Car, it was plausible to suggest that the "high velocity" components in the Hα and Hβ profiles from Car II represent dust scattered profiles from η Car.

In this paper this suggestion is further considered and analysed in the light of new Hα high dispersion, long-slit observations. These data have for the first time allowed the resolution of key spectral features that show that the dust scattering suggestion is correct. The implications of this result on the derivation of a reliable lower limit for the distance to η Car and an insight into the geometry of the region are also discussed.

II. OBSERVATIONS

The observations were made in April 1985 with an echelle spectrograph (Meaburn *et al.* 1984) mounted at the f/7.9 Ritchey-Chrétien focus of the Anglo Australian 3.9-m telescope. In the instrumental configuration used, instead of a cross disperser, a 90 A bandwidth interference filter centered on Hα was used to isolate one echelle order. The detector was the Image Photon Counting System (IPCS) operated on its mode of 1020 channels (= 30 μm each) in the direction of dispersion and 120 x-sections or windows (each = 1.43 arcsec long) along the slit. Two consecutive exposures (1573 and 2000 secs., respectively) were obtained, which covered a line oriented approximately SE-NW (P.A. 132°) crossing from near η Car to the far end of the filamentary ring. The positions of the slits, labeled I and J, are indicated on Figure 1. This figure is sketch of the region contained in Figure 5 (Plate) which is a reproduction from the blue ESO sky survey. In Paper I images of the same region, but in the light of the Hα + [N II] and [S II] ions, were presented; their comparison is worthwhile.

The slit width was set to 70 μm (= 0.5 arcsec) and its length to 171 arcsec. The spectral resolution achieved with this instrumental configuration is 6 km s^{-1} at Hα. The spectra were divided by a Quartz exposure to compensate for instrumental response and calibrated in wavelength with a Cu-Ar lamp. The accuracy of the wavelength calibration is better than $\pm$ 2 km s^{-1}.

A third exposure on η Car, oriented along the same line as in the previous two cases and with the same slit width, was also obtained. These data require a comprehensive description and analysis on their own and their discussion is deferred to López and Meaburn (1986, in preparation). In the present paper only the central, brightest profile along the slit lenght from this exposure is presented in Figure 2 to permit a direct comparison of the shape of the profile from η Car with those from the Car II region.

III. RESULTS

Figures 6 and 7 (Plates) are grey scale representations of the bidimensional data array of the long-slit spectra, corresponding to slit positions I and J, respectively, indicated in Figure 1. These were photographed directly off an "ARGS" image processing monitor unit. The images are in a logarithmic scale in order to show the full intensity range in them with a minimum loss of detail from the faint regions. In both cases the top of the image corresponds to the SW extreme of the slit (x-section 120) and the bottom to the NE end (x-section 1).

Most conspicuous features in these images are the well known splitting ($\sim$ 40 km s^{-1}) of the nebular lines in the region (c.f. Meaburn, López, and Keir 1984 and references therein) and the faint extended ($\sim$ 1000 km s^{-1}) components on both sides of Hα. Also apparent in both images, and of particular relevance, is the absorption component present on the blue side of the main Hα component. Both, the faint extended "wings" of Hα, and the absorption component have been detected along the full length of both frames. Selected regions where the extended components of Hα are more conspicuous have been labeled and their positions have been correspondingly indicated on Figure 1 and Figures 6 and 7 (Plates).

The bright line parallel to the dispersion axis in the upper half of Figure 6 (Plate) corresponds to the continuum from a star marked as "star" in Figure 1. Note also in Figure 6 the dark band crossing nearly at the center of the frame, separating the two brightest extended areas. This is a real feature. It corresponds to the dark bay that defines the famous "keyhole" shape in this region. This result confirms that this dark cloud is actually in front of the H II region, though most probably closely associated to it.

Figure 2 shows the Hα profile from η Car and a profile from position I3. The latter consists of the co-addition of three x-sections and it is presented at an amplified scale in Figure 2 to facilitate comparison with the profile of η Car which is $\sim$ 100 times stronger in this case. Figure 3 displays a mosaic of profiles (again, cuts across the slit length, 5 x-sections co-added) from the positions indicated in Figure 1 and Figures 6 and 7 (Plates).

IV. DISCUSSION

In order to investigate the origin of the "high velocity components" of the Balmer lines in Car II, it is of interest to discuss the principal characteristics of the Hα profile from η Car and their relation to the Hα profiles observed in Car II.

a) *The Shape and Characteristics of the Profiles*

The temporal variability and unique structure in the Balmer profiles of η Car is appreciated by comparing the high resolution Hα profiles of η Car published by Ruiz *et al.* (1984), Melnick, Ruiz, and Maza (1982), Viotti (1985) and Figure 2 in this paper. The Hβ and Hα pro-

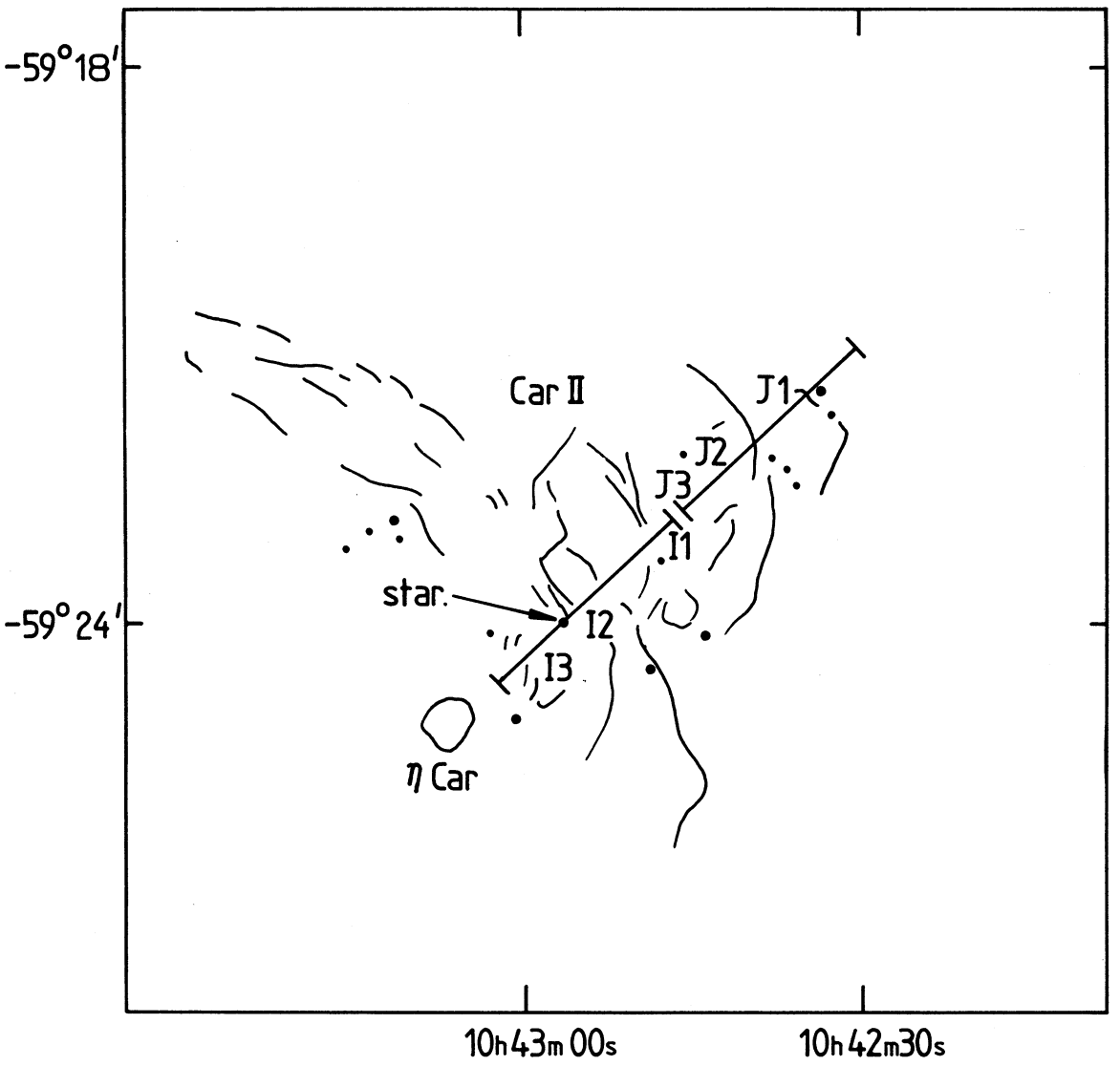

Fig. 1. A sketch of the Car II region and η Car from the blue print shown in Figure 5 (Plate). The position of the slits are included here and regions where the extended components of Hα are most conspicuous are indicated with the labels I3 to J1, according to their position along the corresponding slit. Coordinates are 1950 epoch.

files in Aller and Dunham (1966) are also of interest, as is the Hα profile of Zannela, Wolf, and Stahl (1984).

The high spectral resolution achieved in the present observations allowed for the first time to resolve the fine structure within the "high velocity" components of the Hα profiles from the Car II region. It is apparent from Figure 2 that the overall shape and velocity range of the Hα profile from the I3 region is strikingly similar to the shape of the Hα profile from η Car the main difference being the depth of the absorption component between the profiles of Figure 2.

Maxima labeled as A1 (λ ∿ 6561.5 A) and A2 (λ ∿ 6559 A) by Melnick *et al.* (1982) are indicated in Figure 2 on the profile of η Car. Feature A2 can also be identified in the profile from the I3 region, whereas A1 coincides in this case with the deep blue absorption component. A third maximum on the blue side of the Hα profile of η Car is identified here (λ ∿ 6556.5 A) and has been simply labeled as "A".

A third characteristic of the Hα profile of η Car is its very asymmetric non-gaussian red side of the profile (component E in Melnick *et al.* 1982) with a maximum or shoulder at ∿ 6566.6 A. Components A, A2 and E are detectable in most of the profiles in Figure 3.

A fourth characteristic of the Hα profile of η Car is its very extended red wing, extending in fact in Figure 2

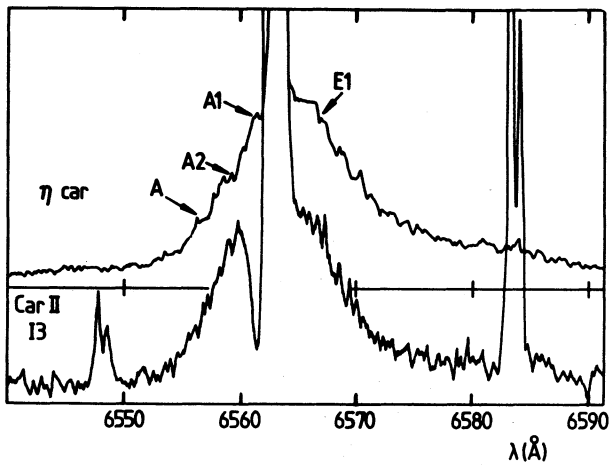

Fig. 2. The amplified Hα profile from the region I3 in Car II and from η Car are shown here together to facilitate comparison. The former profile consists of the co-addition of 3 x-sections along the slit. The similarity of the profiles is remarkable. Maxima labeled in the 1980 Hα profile of η Car by Melnick *et al.* (1982) as A1, A2 and E are indicated here. The feature labeled A is identified in this paper and found to be present, together with A2 and E, all over the face of Car II (see Figure 3). The profile of η Car is ∿ 100 times more intense than the three co-added profiles from region I3.

well beyond the covered wavelength range (note the levels of the continuum on both sides of the profile with respect to the corresponding base lines). This is a real feature, not due to badly corrected instrumental response. This very extended red wing is also clearly present in the coudé spectra of Melnick *et al.* (1982). It is most remarkable that this faint and very extended red wing can also be detected in most of the profiles from the Car II region, up to the most distant slit positions from η Car (see for example the profiles from positions J3 and J2 in Figure 3).

Finally, a fifth unique characteristic of the Hα profile of η Car is its blue shifted absorption component. This component has been presumably formed in the complex expanding circumstellar environment of η Car and is particularly well shown in the profile of March 1982 of Ruiz *et al.* (1984). This blue absorption component is now shown to be present over all the filamentary Car II region (see Figure 3 and Figures 6 and 7, Plates).

The close correspondence of the bright blue nebular patches and filaments with the presence of the extended components of Hα can be readily appreciated by comparing Figure 1 with Figures 5, 6 and 7 (Plates). In these regions the spectral energy distribution of the nebular emission may be expected to be affected by starlight scattered by interstellar dust. In the case of the cloud marked as I3 and I2 in Figure 1 (see also Figure 6) independent proof exists showing that the light of η Car is being scattered within it by dust. This cloud is labeled I1 and I2 in Paper I, where Fe II emission lines from η Car and a steep rise towards the blue in the continuum emission are reported, (see also Walborn and Liller 1977).

These arguments together with the data presented here indicate beyond any reasonable doubt that the filamentary Car II region is reflecting the broad Balmer profiles from η Car. In spite of the intrinsic nebular emission of the region, the scattering effect has become particularly apparent in the Hα emission profile due to the outstanding strength and characteristic shape of the emission from η Car.

The dust scattering mechanism in addition to the temporal variations in the Hα profile of η Car resolve in a natural way the problem of the origin of the very high velocity components present only in the Balmer lines in the Car II region.

b) *The Distance to η Car*

It is pointed out in the previous section that the absorption component in the Hα profile of η Car is only marginally present in April 1985 (Figure 2), whereas this feature is conspicuous in all the Hα profiles from Car II (see Figures 2 and 3). The observations of the Hα profile of η Car indicate that this absorption component has remained practically absent in the previous two or three years. It has diminished in strength from a well defined absorption in early 1982 to a negligible component by March 1983 (Ruiz *et al.* 1984), and it has apparently remained in this state through 1984 (Viotti 1985) and up to at least the last known record to the authors of April 1985, shown in Figure 2. This latest profiles now becomes reminiscent of the 1981 profile presented by Melnick *et al.* (1982). However, it is not known whether or not the distinct changes in the Balmer profiles of η Car are periodic.

Nevertheless, these recent variations in the Balmer emission from η Car and its reflection over the face of the Car II region, represent now a good opportunity to measure directly the distance to η Car and the scattering regions. A situation arises where the Balmer emission profile is having to travel a considerable distance, from ∿ 1 pc for regions I3, to 5 pcs for region J1; adopting a distance to Carina of 2.7 kpc (Turner *et al.* 1980) before being scattered and detected elsewhere. In this conditions the Hα profile observed in, for example, the I3 region of Car II, presented in Figure 2 may be assumed to be the one corresponding to the profile emitted by η Car a few years ago. It is interesting to compare the March 1982 profile of Ruiz *et al.* 1984, with the April 1985 profile of region I3 in Figure 2. Their similarity is absolutely remarkable. Cloud I3, I2 apparently the nearest to η Car, seem then not to have responded yet to the variation in the Hα profile from η Car that occurred between 1982-1983, when the Hα profile lost its conspicuous absorption component. This suggests that this latest known variation of the Hα profile of η Car, is taking at least more than three years to encounter cloud

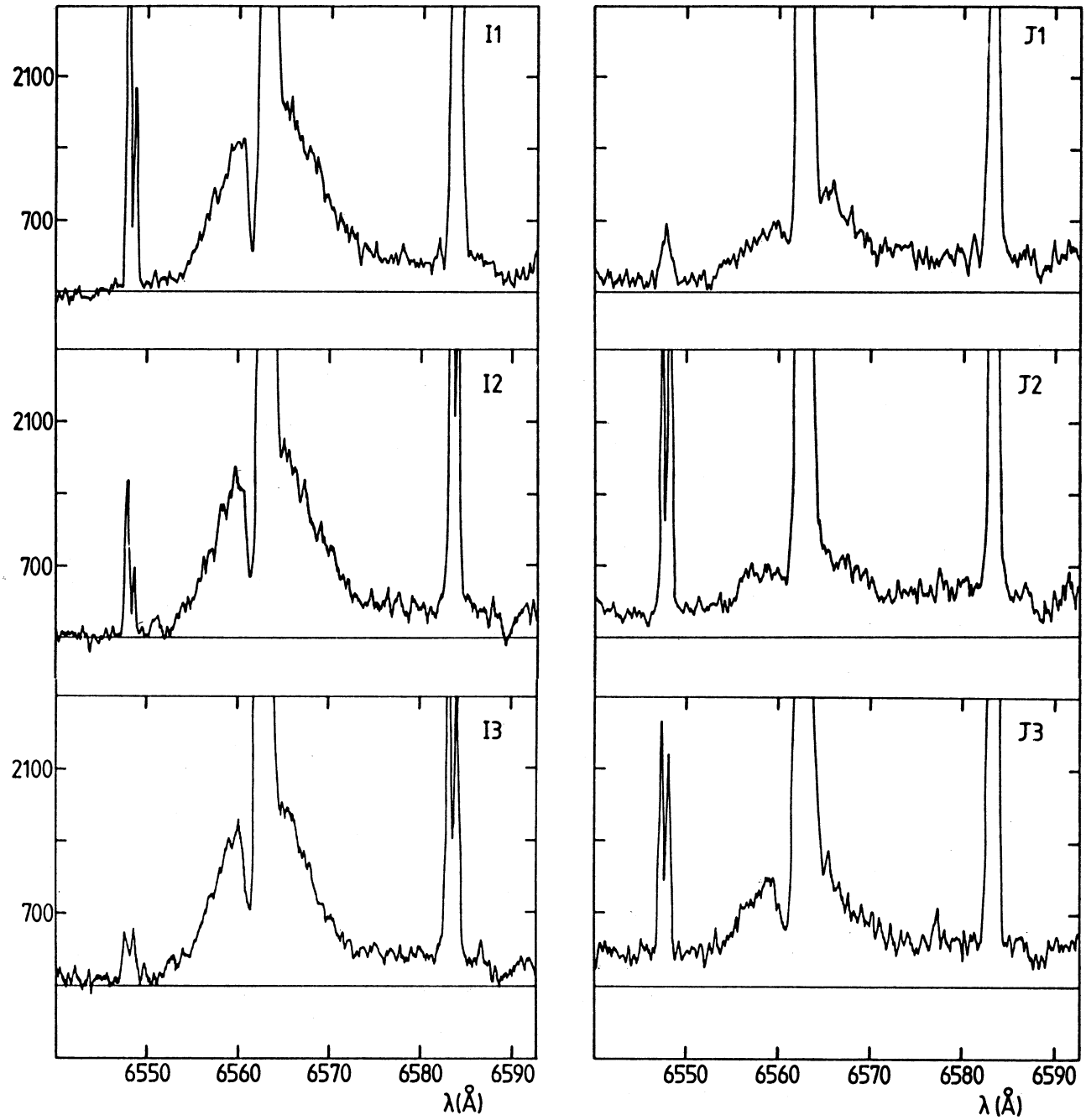

Fig. 3. A mosaic of profiles from regions I3 to J1, indicated in Figure 1 and Figures 6 and 7 (Plates). The profiles consist of 5 x-sections co-added. The persistency of the unique characteristics of the Hα profile from η Car in these profiles that cross all over the filamentary nebulosity, confirms that the Hα emission from Car II is contaminated by scattered Hα radiation from η Car.

I3,I2, which sets a lower limit for the distance of η Car to cloud I3,I2 of ∿ 1 parsec and a corresponding lower limit of ∿ 2 kpc for the Sun – η Car distance.

If a distance Sun-Carina of 2.7 kpc is adopted, then the distance to cloud I3 is ∿ 1.25 pc. Therefore, one should expect to note the corresponding variation on the scattered profile from cloud I3 in 4.08 years. This means that a Hα profile with a very diminished, or absent, absorption component should be observed in cloud I3 between March 1986 and March 1987. Observations monitoring Hα in cloud I3, I2 in the coming months are therefore highly desirable.

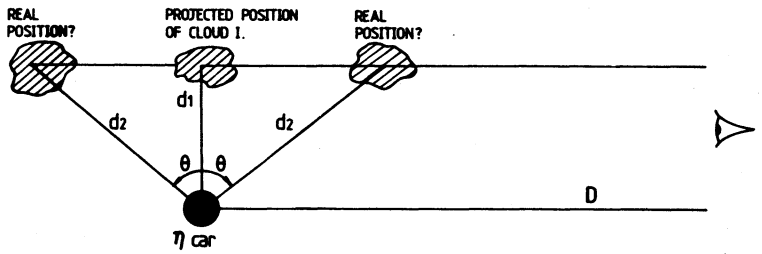

Fig. 4. A simple visualization of the likely geometry of cloud I (regions I3 and I2) with respect to η Car and the line of sight. Cloud I is most probably located either behind or in front of the plane of the sky suggested by d_1. The true distance d_2 from η Car to cloud I is then increased by a factor $d_2 = d_1/\cos\theta$, and the time delay of information traveling from η Car would be given by $\Delta t = d_2/c\,(1-\sin\theta)$. Therefore, the derivation of the distance to η Car from the reflection of its varying Hα profile on cloud I is a true lower limit.

Naturally, the distance that results from measuring the time taken by the varying Hα profile of η Car to be reflected by a cloud in Car II, say regions I3 and I2, hereafter called cloud I, is obtained under the assumption that the projected position of cloud I makes a 90° angle with the line of sight to η Car. If this is not the case, as it is most probable, then the real distance of cloud I to η Car is affected by a $1/\cos\theta$ factor, where θ is the angle subtended between the line that joins η Car to the projected position of cloud I ($\theta = 0$) and the line joining η Car with the real position of cloud I (see Figure 4). Similarly, the corresponding time delay Δt would be given by

$$\Delta t = d_2/c\,(1-\sin\theta)\ ,$$

where c is the velocity of light and d_2 and θ are as in Figure 4. This implies that the distance to η Car obtained by this method represents a true lower limit.

In fact, given the apparent very high efficiency with which Car II is scattering light from η Car and that the lowest efficiency in the scattering mechanism is achieved at a 90° angle, it is reasonable to expect that the Car II region, is located on a plane either behind or in front of η Car, and that a high efficiency multiple scattering mechanism, aided by the apparent high volume density of scatterers in the region, is in operation. The large dimensions of the region together with the brightness of the scattered emission make of Car II an ideal target for a detailed spectropolarimetric and photometric investigation that should surely yield important information on the geometry and physical properties of the scatterers in this outstanding region of massive star formation.

Receipt of an SERC research assistantship by J.A. López while this paper was written at the Astronomy Department of the University of Manchester, is gratefully acknowledged. We also thank the staff at the AAT for their hospitality during the observing trip in April 1985, and Dr. M. Bode for stimulating discussions.

REFERENCES

Aller, L.H. and Dunham, T. 1966, *Ap.J.*, **146**, 126.
Elliot, K.H. 1979, *M.N.R.A.S.*, **186**, 9P.
López, J.A. and Meaburn, J. 1984*a*, *Rev. Mexicana Astron. Astrof.*, **9**, 119.
López, J.A. and Meaburn, J. 1984*b*, *Rev. Mexicana Astron. Astrof.*, **11**, 71.
López, J.A. and Meaburn, J. 1986, in preparation.
Meaburn, J., López, J.A., and Keir, D. 1984, *M.N.R.A.S.*, **211**, 267.
Meaburn, J., Blundel, B., Carling, R., Gregory, D.F., Keir, D., and Wynne, C.G. 1984, *M.N.R.A.S.*, **210**, 463.
Melnick, J., Ruiz, M.T., and Maza, J. 1982, *Astr. and Ap.*, **111**, 375.
Ruiz, M.T., Melnick, J., and Ortiz, P. 1984, *Ap. J. (Letters)*, **285**, L19.
Turner, D.G., Grieve, G.R., Herbst, W., and Harris, W.E. 1980, *A.J.*, **85**, 1193.
Viotti, R. 1985, *The Messenger*, **39**, 30.
Walborn, N.R. and Liller, M.H. 1977, *Ap. J.*, **211**, 181.
Zanella, R., Wolf, B., and Stahl, O. 1984, *Astr. and Ap.*, **137**, 79.

José Alberto López: Instituto de Astronomía, UNAM, Apartado Postal 877, 22860 Ensenada, B.C., México.
John Meaburn: Department of Astronomy, University of Manchester, Manchester M13 9PL, Great Britain.

Rev. Mexicana Astron. Astrof., 13, 33-39 (1986)

SPIRAL STRUCTURE IN THE VELA SECTION OF THE MILKY WAY

E. Irene Vega, J.C. Muzzio, and A. Feinstein

Fac. de Ciencias Astron. y Geofis., Universidad Nacional de La Plata, and
Programa de Fotometría y Estructura Galáctica, CONICET
Argentina

Received 1985 October 9

RESUMEN

En base al análisis de la distribución espacial de estrellas Be (Vega 1982) se estudió la estructura espiral en la zona de Vela. Esta investigación se complementa con un análisis exhaustivo de los distintos indicadores de brazos espirales que han sido observados en la zona por otros autores.

Se establece la presencia de un brazo espiral (el brazo local) aproximadamente tangente a la visual en $\ell = 270°$.. La extensión de dicho brazo es considerable (probablemente alcance unos 6 u 8 kpc del Sol), presentando una pequeña ramificación como la propuesta por Vogt y Moffat (1975). Más allá de la distancia indicada habría una zona interbrazo y, finalmente, se hallan algunos objetos muy distantes que podrían pertenecer a una extensión del brazo +II hacia esas longitudes.

ABSTRACT

The spiral structure in the Vela region is studied through the distribution of Be stars (Vega 1982), and different spiral tracers which had been observed in this zone by other authors. We found that a spiral arm (the Local Arm), is running tangentially along the line of sight at $\ell = 270°$. This arm extends probably in the direction of Vela up to 6 or 8 kpc from the Sun. In addition, it presents a small branch as proposed by Vogt and Moffat (1975). There might be an interarm zone somewhat farther away, and finally, there are some very distant objects that could belong to an extension of the +II arm toward these longitudes.

Key words: GALAXIES-STRUCTURE — SPIRAL STRUCTURE

I. INTRODUCTION

The Vela region, in the southern Milky Way, was one of the least studied zones in the past; it was not attractive enough to look for spiral structure, because as it was considered an interarm region. It also has the disadvantage of being a region of strong absorption which makes it difficult to observed at a large distance from the Sun in the optical range.

More recently, the presence of a spiral arm has been suggested by several authors, notably Herbst (1975), whose argument that at $\ell = 265°$ we are seeing tangentially a spiral arm is based on the fact that the greater absorption is found at $\ell = 270°$, just over the inner edge of the arm delineated by the reflecting nebulae. This would agree with the observations made by Lynds (1970, 1972) who showed that the dust in galaxies concentrates along the inner zone of the optical spiral arms.

One of the most comprehensive works carried out in the zone is perhaps that of Denoyelle (1977) who found that at $\ell = 268°$ there is a relatively strong emission of the local arm up to at least 5 or 6 kpc from the Sun. However, the data he analyzed were not homogeneous. He used spectral types from different authors and he included in his sample stars much later than B2. Besides, he did not attempt to recognize stellar groups. Thus, his diagram of the spiral structure is biased by the distance errors of individual stars and his results might not be trustworthy.

The existence of a spiral arm running tangentially near $\ell = 270°$ is still uncertain. Despite the presence of many tracers of spiral structure in the region, their number is lower than in other zones where spiral arms are known to be present. Among the authors that support this possibility we can mention Humphreys (1979) who proposed that the local arm extends in the direction $\ell = 240°$, suggesting that it may be a branch of the Perseus arm. Georgelin, Georgelin, and Sivan (1979) locate no arm at all in the Vela zone, assigning even the Sun to an interarm zone.

As it can be seen there is great disagreement in relation to the existence of a spiral arm. While some authors suggest that it runs tangentially along $\ell = 270°$, others consider instead this zone as an interarm region.

The present work aims to obtain a clearer picture of the local structure. To achieve this aim a sample of Be stars (Vega 1982) in the regions $266° < \ell < 275°$, $-2.5° < b < 2.5°$ was selected, and in order to include those results into a more general frame, a wider zone was adopted: ($260° < \ell < 280°$, $-5° < b < 3°$) to which observations from others authors were added. The pref-

erence for the negative latitudes is due to the deviation of the optical (Bok, Hine, and Miller 1970) and radio (Kerr and Westerhout 1965) tracers encountered in this direction of the Galaxy.

The Vela region is particularly inadequate for the kinematic derivation of distances due to the slow change of radial velocity with distance. Besides, in view of the criticisms made during the last decade to the use of neutral hydrogen as a spiral tracer and, in particular, of the difficulties involved in the kinematic methods of distance estimation (Burton 1976), it was decided to limit this study to the optical range and to employ radio-astronomical data only as an aid.

II. TRACERS OF SPIRAL STRUCTURE IN THE VELA ZONE

The ratio of total to selective absorption in the 260°-280° region was adopted as R = 3.1 (Barlow and Cohen 1977).

a) *Open Clusters*

The distribution of clusters in the Vela region was studied on the basis of the Janes and Adler (1982) catalogue. Seven clusters were selected with spectral types earlier than B2. This limit insures that the selected clusters are young enough to trace the spiral structure.

b) *OB Stars*

The OB stars in the Vela region were selected from the lists of spectral types of Garrison *et al.* (1977), and the *UBV* photoelectric photometry from Klare and Neckel (1977). For each luminosity class the spectral type was chosen so that the age would not exceed 1.2×10^7 years. This ensures that the stars we selected are young enough. The latest spectral types for each luminosity class are given in Table 1.

TABLE 1

LATEST SPECTRAL TYPE FOR EACH LUMINOSITY CLASS

V	IV	III	II	Ib	Iab	Ia
B2	B4	B5	B6	B9	all	spectral types

Seventy-seven OB stars were found within these limits. The absolute magnitudes given by Crampton and Georgelin (1975) were adopted for stars earlier than B4, and those of Schmidt-Kaler (1982) for the later types; intrinsic colors were taken from Schmidt-Kaler (1982).

Twenty seven OB stars with photoelectric data only were also selected from the lists of Klare and Nekel (1977); in this case only those having $(U-B)_0 < -0.84$ were considered, i.e. stars earlier than B2V according to Schmidt-Kaler (1982).

The results based on *UBV* photometry alone were derived assuming that the stars were of luminosity class V. Their intrinsic colors were obtained using the reddening path $E(U-B)/E(B-V) = 0.72 + 0.05\ E(B-V)$ and the calibration of Schmidt-Kaler (1982). The absolute magnitudes were derived from the intrinsic colors using the zero-age main-sequence calibration of Crampton and Georgelin (1975).

c) *OB Associations*

The new catalog of Ruprecht, Balazs, and White (1981) includes only three probable OB associations in the Vela region; Vela OB1, Vela OB2 and Vela OB3. As the first one is questionable we prefer not to regard it as a real association, but to deal with the H II region RCW38 that could be the nucleus of the assumed association (Muzzio 1979). The two remaining ones are not very useful for this work since Vela OB2 at 460 pc is very near to the Sun according to Brandt *et al.* (1971). The distance of the other one is doubtful, 5000 or 6000 pc, according to Miller (1972 and 1973).

d) *Be Stars*

From the lists of Garrison *et al.* (1977) eleven Be stars were selected, for which we derived the intrinsic colors, and the absolute magnitudes from Schmidt-Kaler (1964*a*, 1964*b*).

Be stars with photometry and without spectral classification were also selected from the list of Klare and Neckel (1977). Their intrinsic colors were obtained in the same way as for the OB stars without spectral classification, but employing the Schmidt-Kaler (1964*b*) calibration for emission-line stars. The absolute magnitudes were taken from the relation derived by Schmidt-Kaler (1964*b*) for color indices $(U-B)_0 < -0.85$.

e) *H II Regions*

A selection of H II regions was obtained from the catalogue of Rodgers, Campbell, and Whiteoak (1960) and of thermal radio sources from the list of Shaver and Goss (1970). Eighteen H II regions were found, two of them, RCW36 and RCW38 related to thermal radio sources.

In some cases it was possible to obtain the radial velocities of H II regions from the work of Georgelin and Georgelin (1970). Their low absolute values show that these regions lie near the Sun according to the Schmidt model (1965). One exception is RCW42, for which Georgelin and Georgelin (1970) using their exciting stars obtained the true distance modulus, $V_0 - M_v = 12.75$ mag.

f) *R Associations*

The three R associations found in the Vela zone were selected from the list of Herbst (1975).

g) *Long-Period Cepheids*

From the lists of Madore (1975) five long-period cepheids (P > 15d) were selected in the Vela zone. Using the mean magnitudes and the periods given by him the color excesses E($B-V$) and the distance moduli were computed for each cepheid by means of the relations given by Tammann (1970).

h) *Wolf-Rayet Stars*

Four WR stars were selected in the Vela zone from the lists of Hidayat, Supelli, and van der Hucht (1981).

III. RESULTS

In what follows we make an analysis of the observations carried out in the Vela zone by different authors. Special emphasis was put on the results from the lists of OB stars of Garrison *et al.* (1977), since they offer the most complete source for the classification of these stars in the southern hemisphere. The open clusters, H II regions, cepheids, R associations, WR stars and the Be stars including those discovered by Vega (1982) will be also presented in § IIIa.

Only three H II regions have been taken into account for the present discussion: RCW 32, RCW 35 and RCW 38. Only for the last one it is available a well determined distance (Bassino *et al.* 1982) from the exciting stars (Muzzio and Celotti de Frecha 1979); RCW 38 is also a giant H II region which provides an excelent spiral tracer. In the remaining H II regions the exciting star is not well determined or, in some cases, the star assumed to be the exciting star is of very late spectral type. This is the case of RCW 42, where Georgelin and Georgelin (1970) assign a B2 IV type, which makes it difficult to believe that it could be the exciting star. For RCW 32 and 35 we adopt the exciting stars suggested by Georgelin and Georgelin (1970) and the spectral types assigned by Garrison *et al.* (1977). These regions have no measurements in the range of 5000 MHz, and perhaps they are not giant H II regions.

Our analysis will consider first the near spiral structure, that is less than 4 kpc, and later on the objects that are located at distances greater than 4 kpc. The former is best determined, but the latter is also of interest despite its inaccuracies.

a) *Spiral Structure up to 4 kpc in the Vela Region*

To begin with, the distribution normal to the galactic plane of all the selected objects was plotted in order to detect any preference for negative latitudes. Figure 1 shows the results from which it is clear that such a preference exists, so that our adoption of a greater interval for the negative latitudes was reasonable.

Figure 2 represents the distribution of the objects in the galactic plane. It shows that for distances less than 2 kpc there is a greater concentration of objects between $260° < \ell < 270°$ with a gap toward greater longitudes. Beyond 2 kpc the distribution becomes more homogeneous.

The distribution of all the objects in longitude and latitude has been represented in Figure 3*a*. It shows a strong concentration toward the range of galactic longitudes $260° < \ell < 270°$. However, if we draw a similar diagram but separating the objects by distance modulus we note that the concentration is more evident for distances less than 2 kpc (Figure 3*b*). At distances greater than 2 kpc there does not appear a tendency of stars to cluster at lower longitudes (260° – 270°), but their distribution looks somewhat more homogeneous (Figure 3*c*). It is then questionable whether this lack of objects between 270° and 280° at distances less than 2 kpc is caused by absorption or to a real lack of a spiral feature.

The plots of the color excesses versus the distance modulus allow us to answer the question mentioned above and to see which is the behavior of the absorption with longitude.

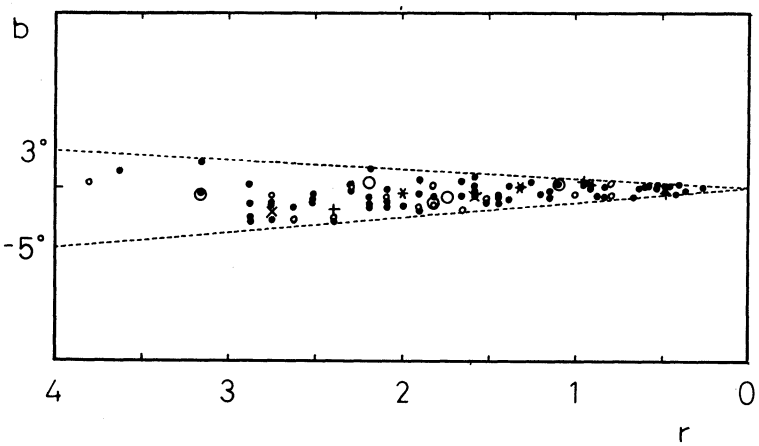

Fig. 1. Spatial distribution up to 4 kpc of: OB stars (dots), Be stars (small circles), H II regions (asterisks), R-Associations (plus signs), young clusters (large circles), Cepheids (crosses), and WR stars (triangles), displayed in a latitude versus distance diagram.

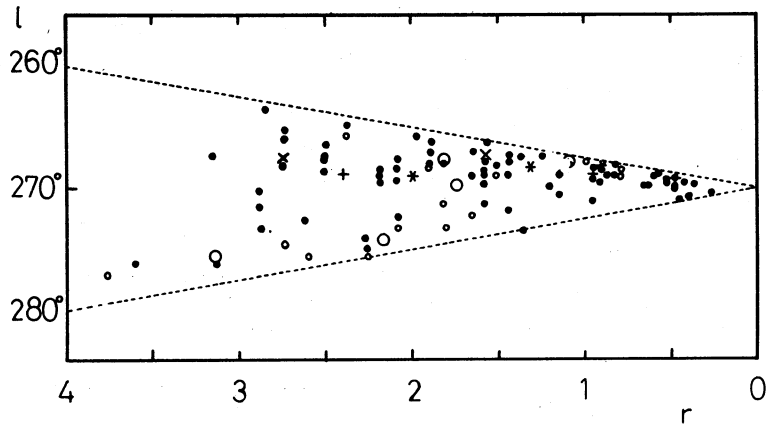

Fig. 2. Spatial distribution of the same objects as in Figure 1, but displayed in a longitude versus distance diagram.

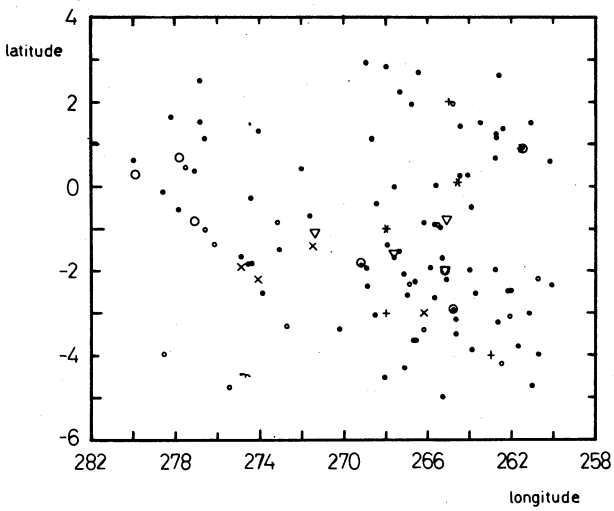

Fig. 3*a* The surface distribution of all the objects. Symbols as in Figure 1.

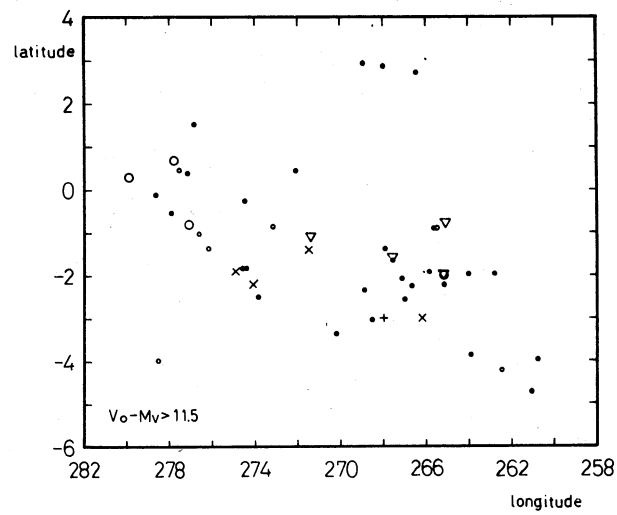

Fig. 3*c*. Same as Figure 3*a*, but for distances greater than 2 kpc.

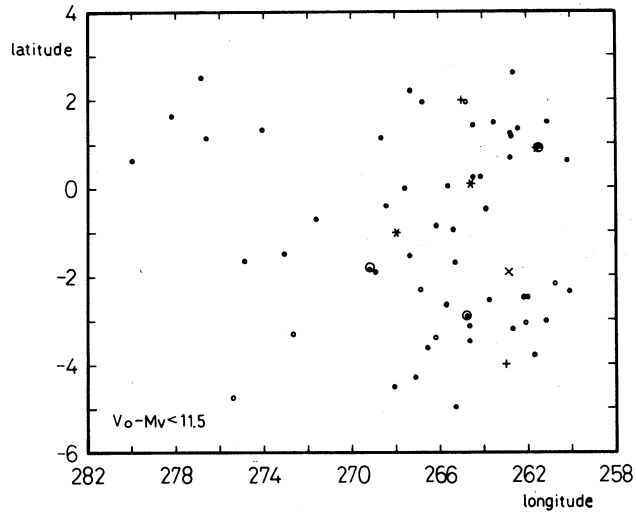

Fig. 3*b* Same as Figure 3*a*, but for distances less than 2 kpc.

The zone under investigation has been divided into four regions with longitude limits of 260°, 265°, 270°, 275° and 280°, and the results have been represented in Figures 4*a,b,c,* and *d*. In addition to the objects presented in the previous figures, there were also included the results from the OB stars of Klare and Neckel (1977), for which only minimum limits of distance can be given. It can be seen that in the region of $260° < \ell < 265°$ (Figure 4*a*) the greatest color excess reaches a value of 1.5 mag at less than 1 kpc from the Sun. At higher longitudes and greater distances there is an increase of the absorption. It is also noticeable that there is a real lack of spiral tracers between $270° < \ell < 280°$ at short distances from the Sun ($r < 2$ kpc).

The high absorption which appears in Figures 4*a,b* and *c* agrees with the results of Stegman and FitzGerald from the Sun. This larger value and the results derived by Lynds (1970), 1972) from other galaxies, suggest

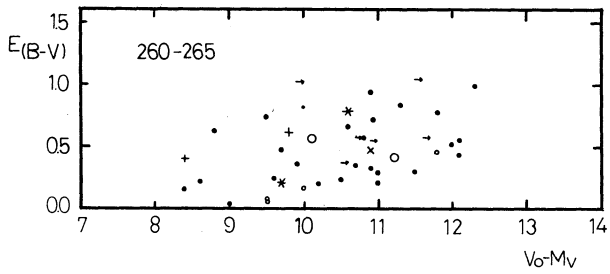

Fig. 4*a*. The diagram of $(B-V)$ color excess versus true distance modulus in the galactic longitude range 260° – 265° of OB stars with photometric data only, are represented with arrows.

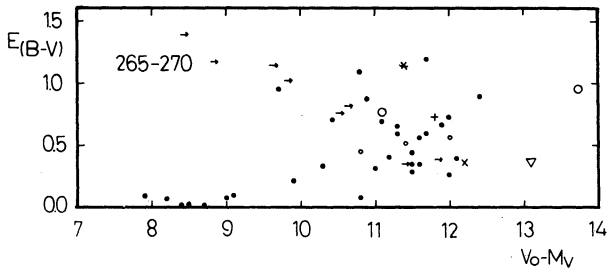

Fig. 4*b*. Same as Figure 4*a*, but for the galactic longitude range 265° – 270°.

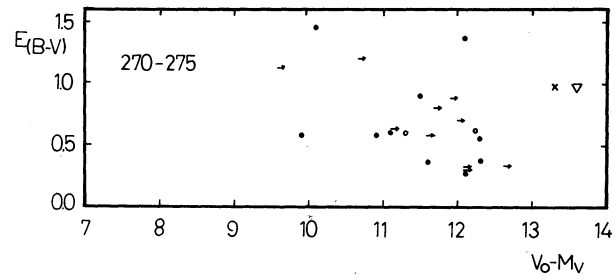

Fig. 4*c*. Same as Figure 4*a*, but for the galactic longitude range 270° – 275°.

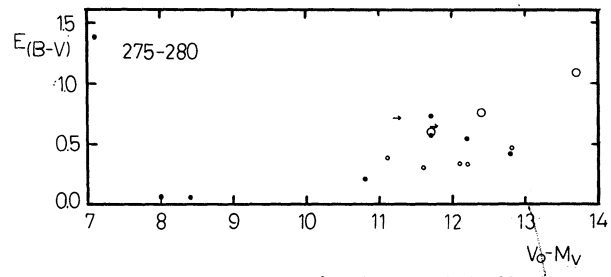

Fig. 4*d*. Same as Figure 4*a*, but for the galactic longitude range 275° – 280°.

that the absorption we found here could be related to the circumstance that we are looking towards the inner part of a spiral arm. This would be the Local Arm which at greater longitudes departs from the ℓ=270° direction.

Bassino *et al.* (1982) carried out a photometric and spectroscopic study of OB stars in a zone between 267° and 272°. Their results confirm the presence of strong absorption relatively near the Sun. A detailed analysis of their own data led these authors to point out that near $l = 267.9°$, $b = -1.5°$, there is a group of stars physically related among them, as well as to RCW 38, an H II region. They derived a distance modulus of $V_0 - M_V = 11.5$ mag (r = 2 kpc) with a mean color excess $E(B-V) = 1.14$ mag. They also give some support to the presence of a farther group (Muzzio 1979) in the same zone, as well as to another one at about 2.5 kpc in the zone $\ell = 272°$, $b = -0.1°$.

The presence of optical tracers which start to be seen at greater distances larger than 2 kpc confirms the above results. This also agrees with our assumption that we are observing a tangent arm, with a dust zone in the inner part of the spiral arm, and with the stellar component behind it.

b) *Spiral Structure Beyond 4 kpc*

The Be stars selected from the lists of Vega (1982), in the zone of completeness (see § I), allow us to derive distances greater than 2 kpc. These stars are plotted in Figure 5 with dots, together with the young clusters, the HII regions, the R-Associations, the Cepheids and the

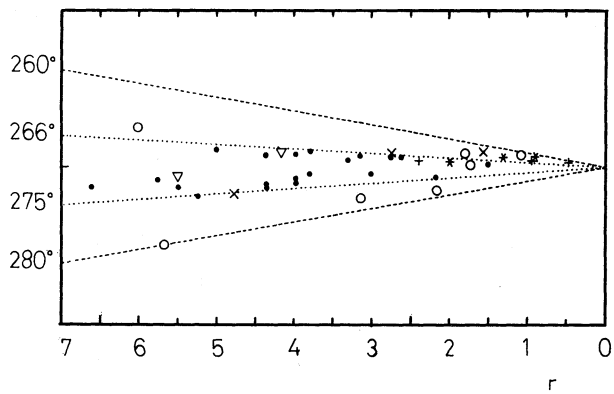

Fig. 5. Spatial distribution up to 7 kpc of: OB stars (dots) together H II regions (asterisks), R-Associations (plus signs), young clusters (large circles), Cepheids (crosses), and WR stars (triangles) displayed in a latitude versus distance diagram.

WR stars. Although, the sample is not very large and the longitude range is small ($267° < \ell < 273°$), it can be noticed that the spiral arm extends even farther away, showing some tendency to curve toward greater longitudes. If tracers up to 16 kpc are included (Figure 6) the Local Arm can be seen distinctly separated from still more distant tracers. The WR stars 12 and 13 and the EZ Vel Cepheid together with two Be stars discovered by Vega (1982), could belong to the extension of the +II arm (Vogt and Moffat 1975). However, it must be taken into account that at such long distances the errors are

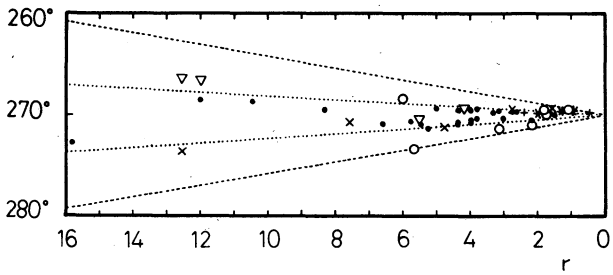

Fig. 6. Same as Figure 5, but for distances greater than 7 kpc.

very large, and our conclusions are thus doubtful. For instance, if we accept that the uncertainty of the distance for a cluster is 15%, it would correspond to an error of 1.5 kpc at a distance of 10 kpc. On the other hand, we have already seen that the limit of completeness for our previous search of Be stars involves distances similar to the value mentioned above. So the gap could be simply caused by the incompleteness of the sample. Nevertheless, the fact that the gap and the appearance of more distant tracers occur also for other tracers, such as the WR and Cepheid stars, suggests the possibility that this phenomenon is real and not a consequence of the incompleteness of the data.

IV. CONCLUSION

The presence in the Vela zone of a spiral arm nearly tangential to the visual has been now well established. There are not only tracers of spiral structure but some of them, as region RCW 38, are conspicuous objects as seen also in other spiral galaxies. Our results show that at greater longitudes the optical tracers of spiral structure appear more distant. If we notice that the same happens with the absorption, which also reaches very high values at distances relatively near to the Sun, then it is reasonable to conclude that we are seeing the arm "from inside" and that it departs from $\ell = 270°$ at greater distances. The extension of the arm is considerable, and it is probably seen in this direction up to about 6 or 8 kpc from the Sun. Because at such distance the arm either bends or ends, we found an interarm zone farther still and perhaps, at even greater distances, part of another arm.

At first sight our results seem to be opposite to some observed facts as well as inconsistent among themselves. Actually, we found an inclination of the arm in the opposite direction to the one observed in the other arms, since they are "open" with respect to a reference circle, while in our case the arm would have such an inclination that would be introduced into the circle. On the other hand, as the width of the arms is of the order of 1 kpc, a typical inclination of about 15° or 18° would imply that our view would not go along over the arm more than about 3.5 kpc at $\ell = 270°$.

Vogt and Moffat (1975) have found at $\ell = 270°$ a branch of the local arm between 1 and 2 kpc from the Sun which perfectly agrees with our conclusions. Since it is just a branch it is not significant that its inclination is opposite to that of the main arms. However, our results allow us to give a more complete model, since to obtain the extension of the spiral tracers found here, it is necessary to see a real arm tangent toward $\ell = 270°$.

There are two reasons to explain why the existence of this arm has not been clearly established in the past. Undoubtedly, the main reason is the enormous absorption present in the zone, even very close to the Sun. Its presence not only prevents the study of the optical tracers, but also their discovery. However, it must also be recognized that the Local Arm, which is the one that extends in Vela, is not delineated by relevant tracers. It is considered by the same authors as a branch of another arm (Yuan 1969), or neglected completely (Georgelin *et al.* 1979) due to the lack of prominent H II regions. Although this last situation is obviously exaggerated in as much as it ignores other tracers different from H II regions, the real fact is that, besides the absorption, their scarcity in the local arm may also contribute to the lack of tracers in Vela.

In conclusion, from this investigation it is found that the Local Arm extends in the direction of Vela up to about 6 or 8 kpc from the Sun, with a small branch as the one proposed by Vogt and Moffat (1975). There would also be an interarm zone beyond that distance and, finally, there are some very distant objects that could belong to an extension of the +II arm toward these longitudes.

We are indebted to R.C. Leonardi, G. Ginestet, S.D. Abal de Rocha, M.C. Fanjul de Correbo, and H. Mosquera for the technical and clerical help. This work was supported with grants from the Secretaría de Estado de Ciencia y Tecnología, the Consejo Nacional de Investigaciones Científicas y Técnicas and the Comisión de Investigaciones Científicas de la Provincia de Buenos Aires.

REFERENCES

Barlow, M.J. and Cohen, M. 1977, *Ap. J.*, **213**, 737.
Bassino, L.P., Dessaunet, V.H., Muzzio, J.C., and Waldhausen, S. 1982, *M.N.R.A.S.*, **201**, 885.
Bok, B.J., Hine, A.A., and Miller, E.W. 1970, in *IAU Symposium No. 38, The Spiral Structure of our Galaxy*, eds. W. Becker and G. Contopoulos (Dordrecht: D. Reidel), p. 246.
Brandt, J.C., Stecher, T.P., Crawford, D.L., and Maran, S.P. 1971, *Ap. J.*, **163**, L99.
Burton, W.B. 1976, *Ann. Rev. Astr. and Ap.*, **14**, 275.
Crampton, D. and Georgelin, Y.M. 1975, *Astr. and Ap.*, **40**, 317.
Denoyelle, J. 1977, *Astr. and Ap. Suppl.*, **27**, 343.
Garrison, R.F., Hiltner, W.A., and Schild, R.E. 1977, *Ap. J. Suppl.*, **35**, 111.
Georgelin, Y.P. and Georgelin, Y.M. 1970, *Astr. and Ap.*, **6**, 349.
Georgelin, Y.M., Georgelin, Y.P., and Sivan, J.P. 1979, in *IAU Symposium No. 84, The Large-Scale Characteristics of the Galaxy*, ed. W.B. Burton (Dordrecht: D. Reidel), p. 65.
Herbst, W. 1975, *A.J.*, **80**, 503.
Hidayat, B., Supelli, L., and van der Hucht, K.A. 1981, *Contributions from the Bosscha Observatory*, No. 68.

Humphreys, R.M. 1979, in *IAU Symposium No. 84, The Large-Scale Characteristics of the Galaxy*, ed. W.B. Burton (Dordrecht: D. Reidel), p. 93.
Janes, K. and Adler, D. 1982, *Astr. and Ap. Suppl.*, **49**, 425.
Kerr, F.J. and Westerhout, G. 1965, *Stars and Stellar Systems*, **V**, 167.
Klare, G. and Neckel, T. 1977, *Astr. and Ap. Suppl*, **27**, 215.
Lynds, B.T. 1972, in *IAU Symposium No. 38, The Spiral Structure of our Galaxy*, eds. W. Becker and G. Contopoulos (Dordrecht: D. Reidel), p. 26.
Lynds, B.T. 1972, in *IAU Symposium No. 44, External Galaxies and Quasi-Stellar Objects*, ed. D.S. Evans (Dordrecht: D. Reidel), p. 56.
Madore, B.F. 1975, *Ap. J. Suppl.*, **29**, 219.
Miller, E.W. 1972, *A.J.*, **77**, 216.
Miller, E.W. 1973, *Bull. A.A.S.*, **5**, 326.
Muzzio, J.C. 1979, *A.J.*, **84**, 639.
Muzzio, J.C. and Celloti de Frecha, M.B. 1979, *M.N.R.A.S.*, **189**, 159.
Rodgers, A.W., Campbell, C.T., and Whiteoak, J.B. 1960, *M.N.R.A.S.*, **121**, 103.
Ruprecht, J., Balazs, B., and White, R.E. 1981, *Catalogue of Star Clusters and Associations*, (Budapest: Akademiai Kiado).
Schmidt, M. 1965, *Stars and Stellar Systems*, **V**, 513.
Schmidt-Kaler, Th. 1964*a*, *Z.f. Astrophys.*, **58**, 217.
Schmidt-Kaler, Th. 1964*b*, *Veroeff. Astr. Inst. Univ. Bonn*, No. 70.
Schmidt-Kaler, Th. 1982, *Landolt-Bornstein, New Series* VIb/2.
Shaver, P.A. and Goss, W.M. 1970, *Australian J. Phys. (Astrophys. Suppl.)*, **14**, 133.
Stegman, J.E. and FitzGerald, M.P. 1972, *Royal Astron. Society of Canada Journal*, **66**, 303.
Tamman, G.A. 1970, in *IAU Symposium No. 38, The Spiral Structure of our Galaxy*, eds. W. Becker and G. Contopoulos (Dordrecht: D. Reidel), p. 236.
Vega, E.I. 1982, *A.J.*, **87**, 794.
Vogt, N. and Moffat, A.F.J. 1975, *Astr. and Ap.*, **39**, 477.
Yuan, C. 1969, *Ap. J.*, **158**, 871.

Alejandro Feinstein, Juan C. Muzzio, and E. Irene Vega: Observatorio Astronómico de La Plata, Paseo del Bosque s/n 1900 La Plata, Provincia de Buenos Aires, Argentina.